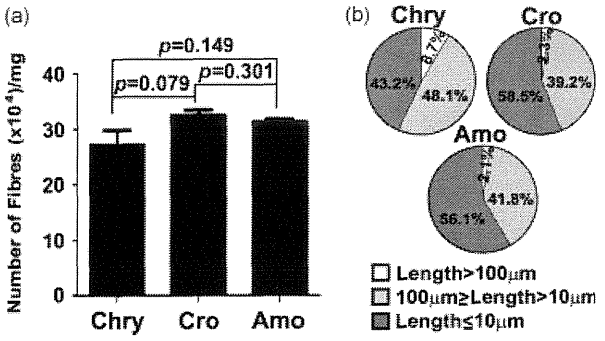

Figure 1. Characteristics of UICC asbestos fibres. (a) Number of fibres per weight (means ± SEM; $N = 15$). (b) Fraction of long and short fibres. Chry = chrysotile; Cro = crocidolite; Amo = amosite.

for unequal variances when necessary; Fisher's exact test; and the chi-square test. $p < 0.05$ was considered statistically significant.

Results

Re-evaluation of UICC-grade asbestos fibres

Three kinds of standard asbestos fibres obtained from Unio Internationalis Contra Cancrum (UICC) were re-evaluated. The number of fibres per weight was not significantly different among the three groups of asbestos fibres (Figure 1a). Chrysotile contained a higher fraction of longer fibres than those of the other two asbestos types (Figure 1b).

Comparison of mesothelial carcinogenesis by three different asbestos fibres and its modification by an iron chelator, NTA

We injected chrysotile, crocidolite or amosite fibres (10 mg; UICC) into the peritoneal cavity of F_1 hybrid rats from crosses of the Fischer-344 and Brown-Norway strains (Figure 2a). MM developed and infiltrated diffusely, concomitant with massive bloody ascites (Figure 2b) in 96.9% (94/97) of the rats injected with asbestos within 800 days after injection (Supplementary Table 1). Progression of the disease was fatal, due to malnutrition and organ failure via invasion (Figure 3a). We did not observe MM in two (2/41) rats of the crocidolite group and one (1/28) rat of the amosite group, which was confirmed histologically after sacrifice at day 812. Here, tangled CNTs, found to be non-carcinogenic [13], were included as a negative control of foreign fibrous material (Figure 2c). NTA alone does not induce MM, as described by us [14] and other investigators [22,23].

There are three distinct histological subtypes of MM: EM; SM; and biphasic mesothelioma (BM; a hybrid of EM and SM; Figures 2d and 3a). To confirm the mesothelial lineage of the tumours, we performed immunohistochemical analyses [Figure 3b, upper panel; positive for cytokeratin, calretinin, podoplanin (D2-40), and mesothelin; negative or weakly positive for desmin and S100]. SM revealed weaker cytokeratin, no calretinin, and no podoplanin, but intense mesothelin immunostaining. The immunohistochemistry results in tissue array samples are summarized in the lower panel of Figure 3b. Results of western blot analysis (podoplanin and calretinin) were positive for both types, albeit low positivity in SM (Figure 3c). Serum mesothelin at day 420/480 was significantly higher in the rats injected with asbestos than in control rats (Figure 3d).

We found that chrysotile fibres of the same weight caused a significantly shorter survival of rats via MM induction in comparison to crocidolite and amosite fibres (Figure 2c). Furthermore, we observed a higher frequency of SM in the chrysotile group, despite lack ($p = 0.111$ versus amosite) of statistical significance (Figure 2d). SM showed a significantly poorer prognosis than EM (Supplementary Figure 1). These results suggest that chrysotile fibres induce more aggressive disease than the other two fibres.

Chronic iron overload has been associated with carcinogenesis [24,25]. To evaluate the role of iron in asbestos-induced mesothelial carcinogenesis, we administered NTA, an iron chelator, to promote the Fenton reaction [26], to ~50% of the animals of each group (Supplementary Table 1). Unexpectedly, repeated weekly administration of NTA significantly accelerated mesothelioma development, not only in the crocidolite and amosite groups but also in the chrysotile group (Figure 2e). Males showed a faster progression of disease when treated with chrysotile fibres (Figure 2f), suggesting the influence of sex hormones either on the iron metabolism or on anti-oxidative mechanisms, as in the case with ferric NTA [27].

NTA promotes oxidative DNA modification in a sub-acute study

The ability of NTA to potentiate oxidative stress caused by asbestos fibres was tested in a sub-acute study of 3 weeks. Animals received intraperitoneal injection of 5 mg of chrysotile or crocidolite. Two weeks later, half of the animals received 80 mg/kg NTA and were killed after 24 h. Immunohistochemical analysis of 8-OHdG revealed that nuclear staining of mesothelia after asbestos and NTA is much stronger, with stromal oedema, than that of asbestos and a vehicle saline (Figure 4).

Association of local iron overload in asbestos-induced mesothelial carcinogenesis

To confirm the iron involvement in asbestos-induced mesothelioma, we performed Perl's iron staining of each of the abdominal organs collected from rats with MM in each asbestos group. The staining revealed prominent iron deposits in the spleen, liver, and kidney including surface mesothelial cells of rats injected with asbestos, whereas iron deposits were minimal in the age-matched controls (Figure 5a). Additional NTA treatment groups showed higher iron accumulation than

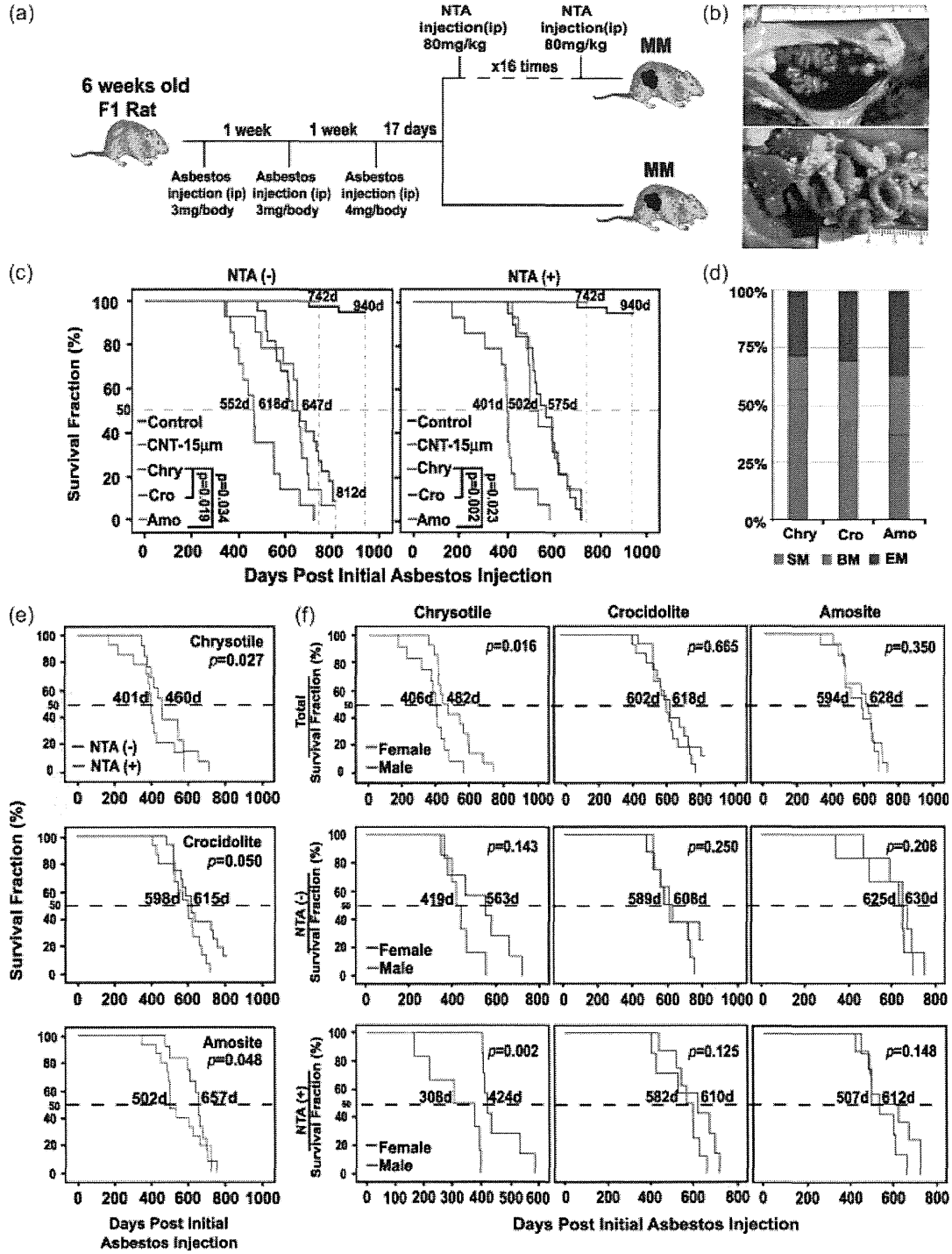

Figure 2. Induction of lethal peritoneal mesothelioma by three commercially used types of asbestos. (a) Carcinogenesis protocol. NTA = nitrilotriacetic acid, a synthetic iron chelator to promote the Fenton reaction; ip = intraperitoneal; MM = malignant mesothelioma. (b) Typical case of MM. Bloody ascites (upper panel) and multiple whitish tumours all over the peritoneum (lower panel). (c) Survival fraction regarding asbestos type. All the deaths were due to MM, except those in the untreated control group (see Supplementary Table 1 for details). Nanotube = tangled multi-walled carbon nanotube (diameter ϕ = 15 nm); d = days. p values for Kaplan–Meier analysis were calculated by the log-rank test. See text for details. (d) Ratios of histological type (EM = epithelioid mesothelioma; BM = biphasic mesothelioma; SM = sarcomatoid mesothelioma). (e) Survival fraction regarding asbestos type and NTA administration. (f) Survival fraction regarding asbestos type, sex, and NTA administration. See the Materials and methods and Results sections for details.

groups of asbestos alone. No iron accumulation near mesothelial cells was observed with tangled multi-walled CNTs that do not induce carcinogenesis. A detailed comparison of a variety of CNTs has been published elsewhere [13]. Iron measurements of the spleen and liver corroborated the results of Perl's iron staining, revealing significantly higher levels in all the asbestos groups than in the controls, which were further increased with additional NTA (Figure 5b). Serum from the 11 chrysotile-treated, 11 crocidolite-treated, and 15 amosite-treated rats 420 days after asbestos injection showed significantly higher levels of serum

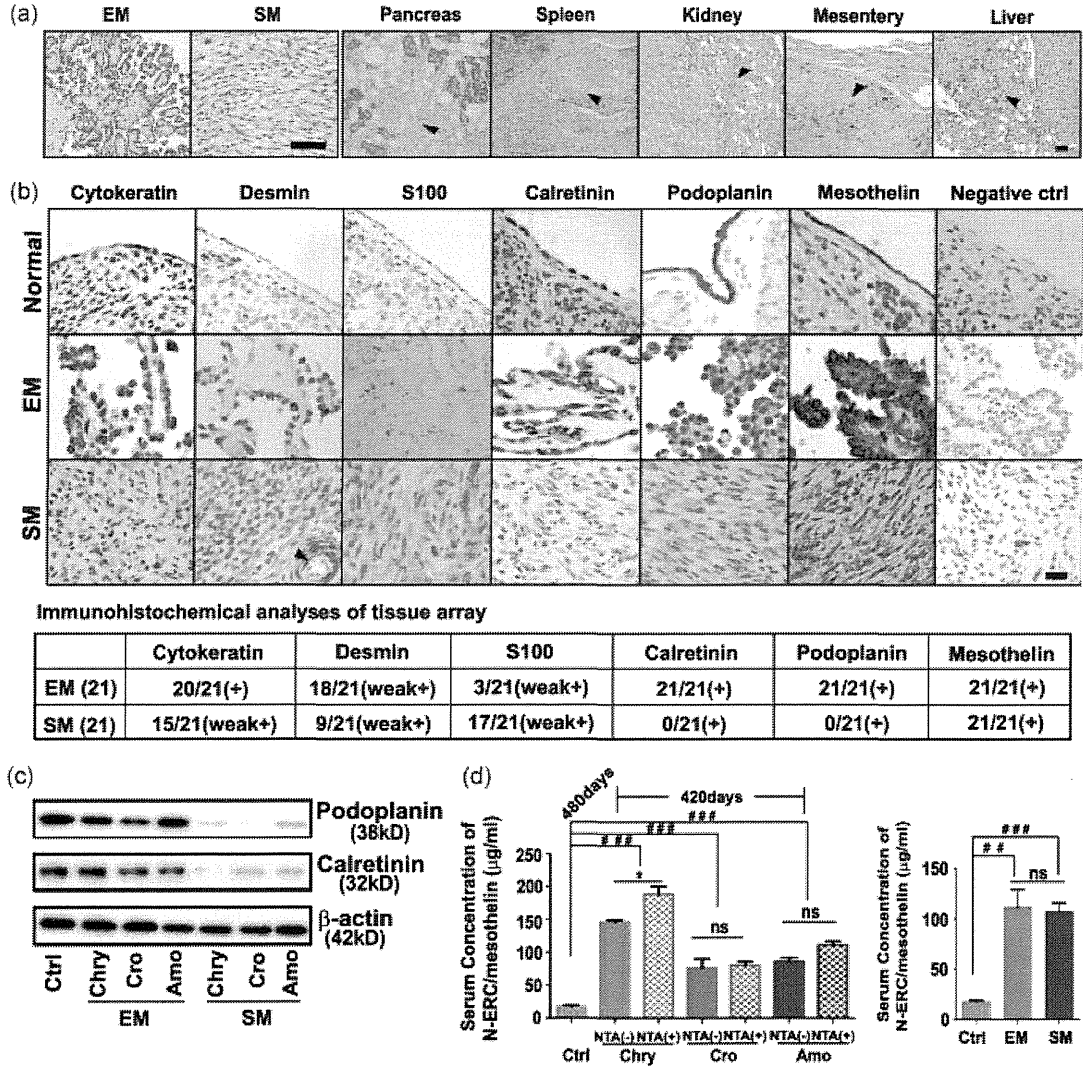

	Cytokeratin	Desmin	S100	Calretinin	Podoplanin	Mesothelin
EM (21)	20/21(+)	18/21(weak+)	3/21(weak+)	21/21(+)	21/21(+)	21/21(+)
SM (21)	15/21(weak+)	9/21(weak+)	17/21(weak+)	0/21(+)	0/21(+)	21/21(+)

Figure 3. Characteristics of asbestos-induced peritoneal mesothelioma in rats. (a) Histology of malignant mesothelioma. Invasion (arrowheads) is prominent in various organs (EM = epithelioid mesothelioma; SM = sarcomatoid mesothelioma; bar = 100 μm). (b) Immunohistochemical analysis for the evaluation of mesothelial origin (bar = 50 μm). The brown colour is the positivity except podoplanin (pink). Normal, rat control surface mesothelial cells; negative controls (ctrl) are shown as procedures without primary antibody (arrowhead, smooth muscle in a vessel). The inset table summarizes the immunohistochemical results. (c) Western blot analysis of the tumours. (d) Serum mesothelin (N-ERC; antigen at N-terminal portion) before apparent recognition of tumours (means ± SEM; $^{\#\#}p < 0.01$, $^{\#\#\#}p < 0.001$ versus untreated control; $^{*}p < 0.05$ between NTA(+) and NTA(−) in the same fibre group; ns = not significant). See the Materials and methods and Results sections for details.

ferritin than the controls, which was further increased with additional NTA (Figure 5c, left panel). We also measured the serum levels of NTBI, which revealed that the serum levels of NTBI were substantially reduced in the rats of the asbestos groups compared with the controls (Figure 5c, right panel), suggesting that a mechanism worked to withdraw 'catalytic' iron from serum.

Characteristics of iron metabolic pathways in asbestos-induced MM

We further examined the expression levels of genes associated with iron metabolism in MM. *DMT1* (*SLC11A2*) and *transferrin receptor 1* (*Tfrc*) are the genes involved in the uptake of iron from the extracellular compartment into the cells and its utilization, whereas *ferroportin 1* (*SLC40A1*) is involved in its export out of cells [28]. We found that the expression of *DMT1* and *Tfrc* was up-regulated in the MM tissues, whereas expression of *ferroportin 1* (Figure 5d) and *Dcytb* (duodenal cytochrome b; Supplementary Figure 3a) was down-regulated. Increased expression of *DMT1* in the mesothelioma samples was further confirmed by immunohistochemical staining (Supplementary Figure 2).

Evaluation of mesoderm-specific transcription factors

Two mesoderm-specific transcription factors (*Dlx5* and *Hand1*) were activated (Figure 5e). Among the expression levels of ectoderm- and endoderm-specific transcription factors, *Isl1*, *Pax6*, and *Mels1* were also increased in the mesothelioma samples; however, the increase was not prominent (Supplementary Figure 3).

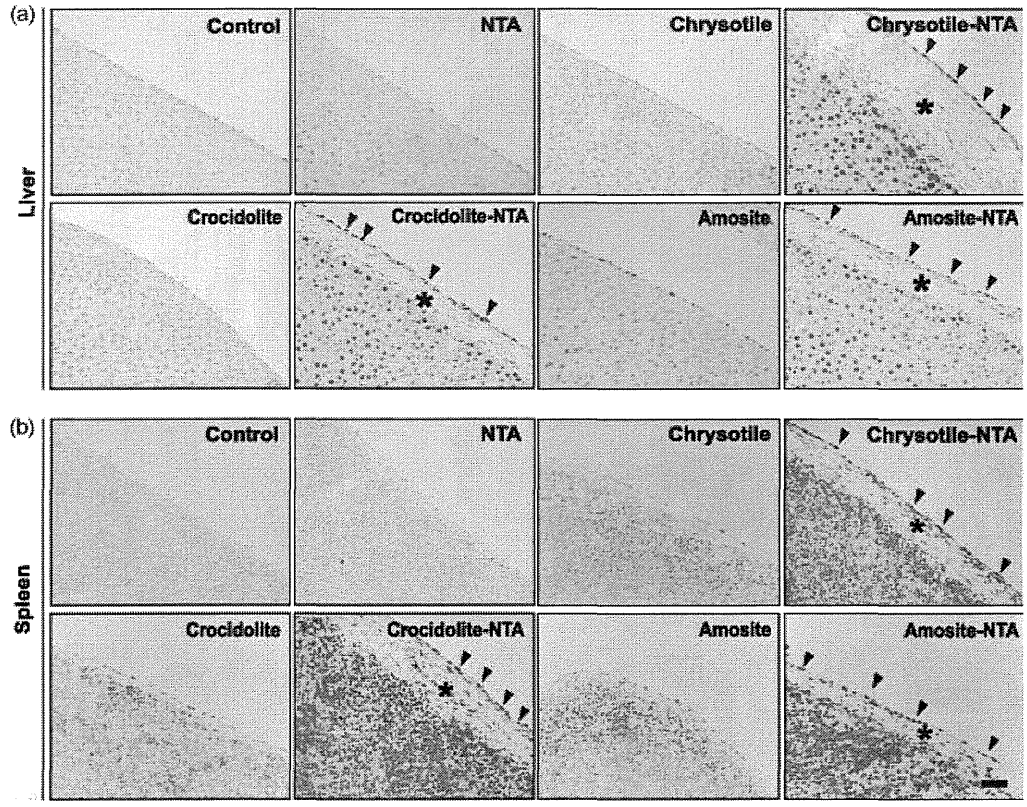

Figure 4. Immunohistochemical analysis of an oxidized DNA base, 8-hydroxy-2′-deoxyguanosine (8-OHdG) after treatment of asbestos followed by NTA. NTA (80 mg/kg) was administered intraperitoneally 2 weeks after ip administration of each asbestos fibre (5 mg). Note the nuclear positivity of mesothelial cells on the surface of (a) the liver and (b) the spleen. Representative figures are shown (bar = 50 μm). NTA enhanced the nuclear 8-OHdG positivity of the mesothelial cells, following different asbestos exposures (arrows, intensely stained nuclei of mesothelial cells; asterisk, oedema).

Genomic alterations in asbestos-induced MM

We then investigated the chromosomal aberrations in rat asbestos-induced MMs using the aCGH method (GEO accession: GSE36577). The results showed substantial genomic alterations over the whole genome, with many gains and losses of large chromosomal fragments (Figure 6a and Supplementary Figures 4a, 4b, and 5a). Many of the genomic alterations were not in common for each MM. However, high-copy amplification over a wide region of chromosomes 7 and 12 was observed in common, and deletion of genes across a wide region of the chromosome was observed in chromosomes 5 and 8 (Supplementary Figures 4a–4d). Chromosomal deletions in chromosomes 5 and 8 occurred more frequently in chrysotile-induced MMs (Supplementary Figure 4c), but encompassed narrower chromosomal regions globally in the genome in the chrysotile-induced MMs (Figure 6b). We found a common chromosomal deletion mapped to the chromosome 5q32 locus, containing the genes encoding the tumour suppressor genes *CDKN2A/2B/ARF*. Homozygous deletion of *CDKN2A/2B/ARF* was observed in the majority (92.6%; 25/27) of the rat MM samples, independent of the type of asbestos fibres used (Figure 6c). Loss of the *CDKN2A/2B/ARF* gene was confirmed by fluorescence *in situ* hybridization and quantitative real-time PCR analyses (Figures 6d and 6e). Furthermore, although we did not observe any change in the gene copy number of the two tumour suppressors *p53* and *NF2*, we found significant down-regulation in the expression levels of these two genes in the majority of the rat mesothelioma samples (Figure 6f). Such findings indicate that in addition to CDKN2A/2B/ARF and p53, loss of NF2 is also closely associated with MM development, although the loss of the NF2 pathway is likely to occur via epigenetic mechanisms. The three asbestos types were not differentiated with hierarchical clustering of the aCGH results.

Copy number changes associated with different histologies

As noted above, histologically, MMs can be classified into three distinct forms. We compared the aCGH results of these three different subtypes and found that SM showed the highest degree of genomic instability ($p < 0.05$) compared with the other subtypes (Supplementary Figures 5a and 5b). We also noticed that BM shows a frequent gain of gene copy number in chromosome 8, mapping to the region containing oncogenes such as *Birc2, Birc3*, and *YAP1* [29] (Supplementary Figure 5c). In addition, SM also had a more frequent amplified region in chromosome 7, which includes genes such as *Cct2* [30] and *Lyz* [31] (Supplementary Figure 5d).

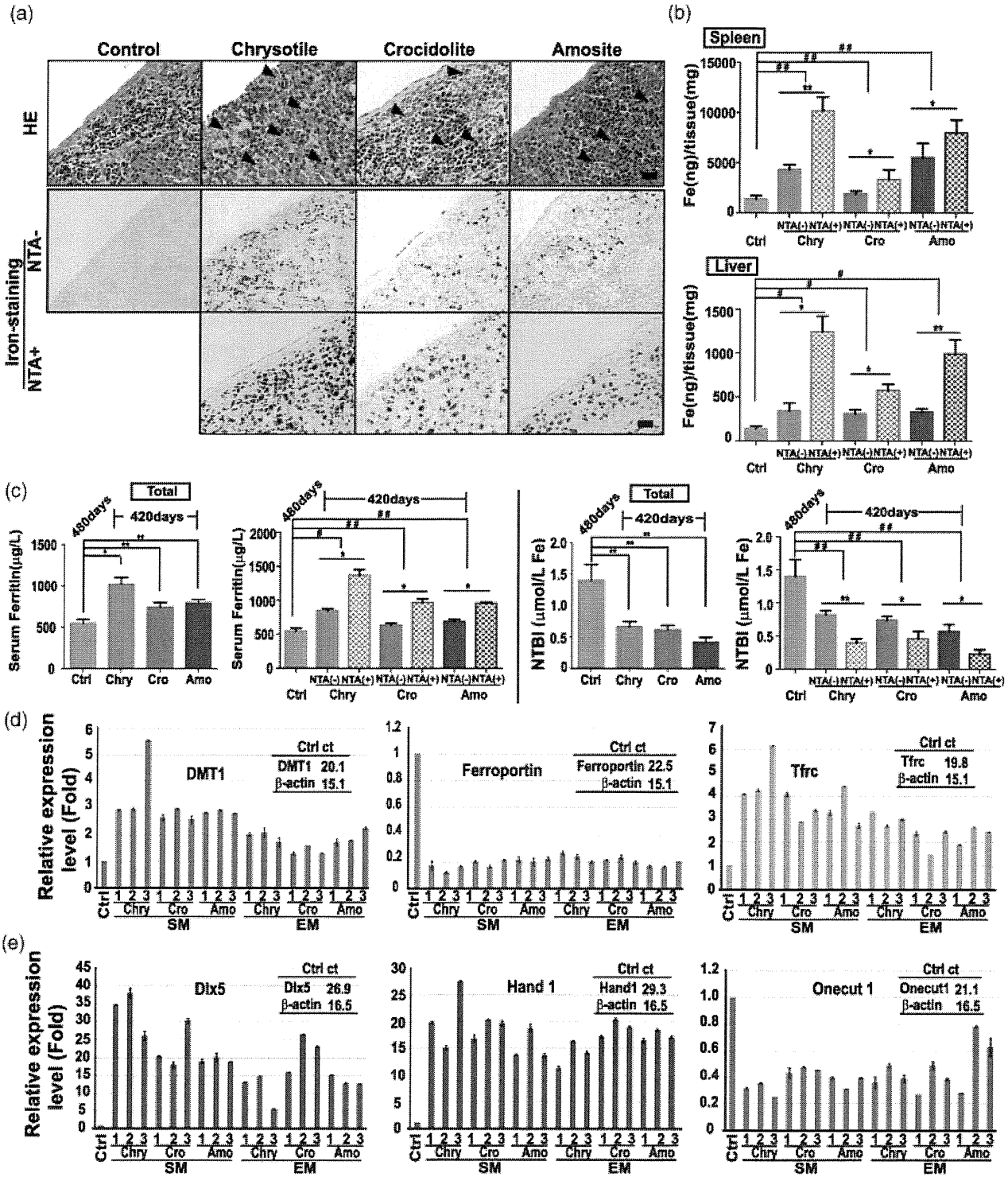

Figure 5. Iron overload in asbestos-induced mesothelial carcinogenesis and gene regulation in asbestos-induced mesothelioma. (a) Prominent deposition of iron in the spleen and mesothelial cells (upper row, haematoxylin and eosin staining; arrowheads, hemosiderin deposits; lower row, Perl's iron staining; bar = 100 μm; 50 μm in the insets). (b) Iron concentration in various organs of the peritoneal cavity regarding asbestos type and NTA administration (means ± SEM; $N = 5$ randomly selected among sacrificed animals after day 420). (c) Serum ferritin and NTBI (non-transferrin-bound iron) before apparent recognition of tumours (means ± SEM; $N = 5-12$). See Supplementary Table 1 for details. (d) Expression of iron-associated genes in the asbestos-induced mesothlioma. *DMT1, SLC11A2; ferroportin, SLC40A1; Tfrc, transferrin receptor 1* (CD71); Ctrl ct, control cycle times. Ctrl is the control mesothelial sample obtained by scraping rat solid organs as described in the Materials and methods section (means ± SD, triplicate). (e) Expression of mesoderm-specific transcription factors in the asbestos-induced mesothelioma. Sample numbers correspond to each other in d and e (means ± SD, triplicate).

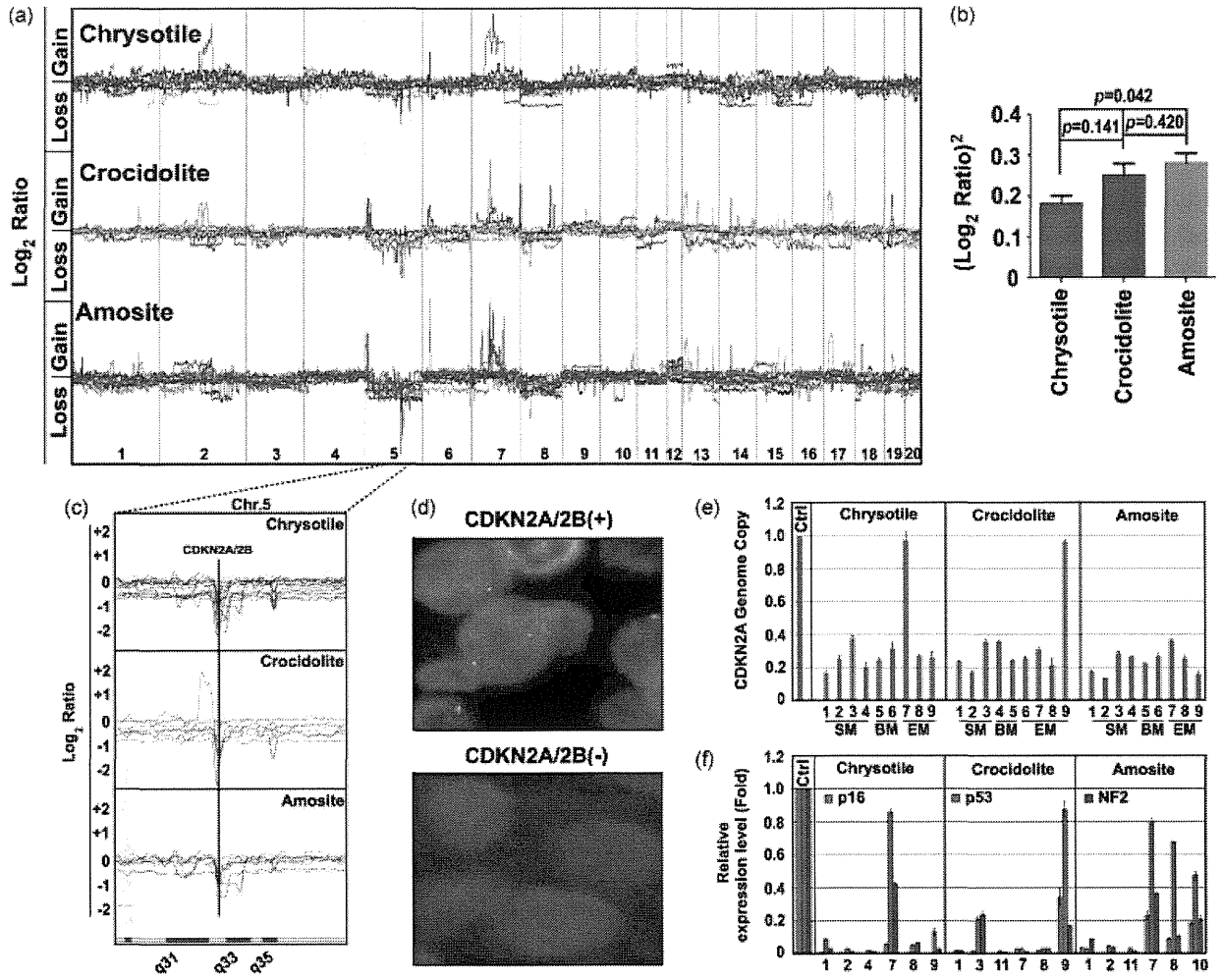

Figure 6. Massive genomic alteration with homozygous deletion of *CDKN2A/2B* is a hallmark of asbestos-induced mesothelioma. (a) Combined scheme of array-based comparative genome hybridization analysis ($N = 9$ for each asbestos, consisting of 3 EMs, 2–3 BMs, and 3–4 SMs, respectively). The three asbestos types were not differentiated with hierarchical clustering. (b) Quantitation of chromosomal aberration over the whole genome by ($\log_2$ ratio) [2]. Zero means no amplification/deletion (2N state), and the increased number indicates amplification/deletion with the same weight between 4N amplification and N (heterozygous) deletion (means ± SEM; SM, $N = 10$; BM, $N = 8$; EM, $N = 9$). (c) Homozygous deletion of *CDKN2A/2B* is observed in 25/27 cases (88.9% in chrysotile- or crocidolite-induced mesothelioma; 100% in amosite-induced mesothelioma). (d) Fluorescence *in situ* hybridization analysis to confirm the homozygous deletion of *CDKN2A/2B*. Pink dots are the signals under DAPI nuclear counter-staining. (e) Semi-quantitative PCR analysis for evaluation of the copy number of the *CDKN2A/2B* locus (means ± SD, triplicate). (f) Expression of *CDKN2A* (*p16*), *p53*, and *NF2*. Sample numbers correspond to each other in e and f (means ± SD, triplicate).

Discussion

Many animal experiments were performed regarding the carcinogenicity of asbestos in the 1970s and 1980s [1]. One of the fruitful outcomes was 'Stanton's hypothesis' on macrophage involvement that asbestos fibres longer than 8–20 μm and thinner than 0.25 μm more readily induce MMs [32,33]. The present experiments are a re-evaluation of those with modern molecular techniques under specific pathogen-free environments in the hope of understanding, preventing, and curing asbestos-induced mesothelial carcinogenesis. We also re-evaluated the UICC standard asbestos fibres reportedly produced in the 1990s and found that the fibre numbers per weight were not significantly different among the three commercial asbestos types, but that chrysotile contained a higher fraction of long fibres (Figure 1). We cannot rule out the possibility that a high fraction of longer fibres affected the carcinogenicity, but these are the standard types of asbestos used in the scientific community.

MMs induced in rats were similar to their human counterparts histologically as well as immunohistochemically [34], and from the standpoint of serum marker [35,36] (Figure 3). The data presented here point towards the idea that chrysotile is the fastest to induce MM among the commercial types of asbestos, with a higher fraction of a more malignant SM type (Figure 2 and Supplementary Figure 1). Although chrysotile itself contains a small amount of iron, iron overload appears to have played an important role in chrysotile-induced mesothelial carcinogenesis, as did crocidolite and amosite. Furthermore, the iron-overloaded condition was most prominent with chrysotile, as seen by iron staining, measurements, and serum ferritin levels (Figure 5). This is presumably via

its high haemolytic activity and the associated catalytic activity of iron, making the surface of asbestos a niche for oxidative modification [37], and is consistent with the cultured cell experiments using iron-loaded synthetic chrysotile [38]. Interestingly, the genomic aberration area was narrower than the other two types of asbestos (Figure 6b), suggesting that chrysotile attack is more pinpoint and is in the proximity of genomic DNA. This pathogenic mechanism of iron involvement was demonstrated further by the significant promotional effect of NTA (Figure 2f) and by the characteristic pattern of genomic alterations (Figure 6c) in the iron-induced rat tumours [39]. No iron accumulation, in our recent publication [13], near mesothelial cells with tangled CNT (no MM formation; Figure 2c) confirms the involvement of iron overload in mesothelial carcinogenesis.

NTA, a synthetic aminopolycarboxylic acid, binds with hydrogen bonding only three or four out of six ligands of ferric iron, thus leaving free catalytic ligands at neutral pH [40]. We showed that even a single intraperitoneal injection of NTA enhanced the *in vivo* oxidative DNA modification of mesothelial cells 2 weeks after asbestos administration (Figure 4). The significantly earlier occurrence of MM in male rats than in females only in the chrysotile group (Figure 2f) may result from the sex difference in iron metabolism and suggests a strong commitment of iron overload in chrysotile-induced carcinogenesis.

In animal models without genetic engineering, homozygous deletion of *CDKN2A/2B/ARF* is observed only in ferric-NTA-induced renal cell carcinoma of rats [41] and in sarcomatoid mesothelioma of rats induced by ferric saccharate with NTA [15,39], as far as we know. Therefore, we believe that this genetic alteration represents an 'iron overload' signature. The present data strongly support the role of iron overload in chrysotile-induced carcinogenesis. This aberration causes simultaneous loss of both the RB and the p53 (via ARF) tumour suppressive pathways [39]. Since this is a most frequently observed genomic alteration in human MMs [42], this rat model precisely mimics human MMs. Hierarchical clustering did not detect an asbestos-specific difference in the array CGH profiles, though we found a tendency of more frequent chromosomal deletions in chromosomes 5 and 8 but globally narrower chromosomal aberration in chrysotile-induced MMs (Figure 6 and Supplementary Figure 4). Inclusion of *Yap1* amplification (Supplementary Figure 5c) in the Hippo pathway [43] confirms that the present rat model is similar to the human counterparts. Recently, an aCGH analysis of murine MM (*NF2*$^{+/-}$ and wild-type) cell lines was reported although a low-density BAC CGH array was used. Alteration of *CDKN2A* and *CDKN2B* was observed at 56% and 60%, respectively [44]. Their study does not rule out the possibility of a deletional event during the establishment of cell lines as described previously [45].

We observed that there was a tendency for iron to accumulate in cells (macrophages, mesothelial cells, and other parenchymal cells) after exposure to each asbestos type, concomitant with low serum NTBI (Figure 5). This precisely mimics the inflammatory condition caused by bacterial infection, where the host undertakes to deprive bacteria of available iron [46]. Of note, an iron regulatory profile of this kind was also observed in the asbestos-induced MMs (Figure 5d).

Based on direct and indirect evidence, we propose that the iron overload condition is the key pathological condition during mesothelial carcinogenesis by all the commercially used asbestos types. Therefore, iron modulation via phlebotomy, iron chelators or any other means to remove local excess iron might be a hopeful strategy for preventing MM.

Interestingly, we found that asbestos-induced MMs are driven by the mesoderm-specific transcription factors DLX5 [47] and HAND1 [48], but not by ONE-CUT 1 (HNF6) [49] (Figure 4e). DLX5 expression was much stronger in the asbestos-induced MM than that induced by iron saccharate, but an ectoderm-associated transcription factor, PAX 6, was commonly overexpressed (Supplementary Figure 4c) [15].

The major limitation of our study is that intraperitoneal administration differs from the situation of human environmental exposure. We understand that present experiments evaluated the carcinogenicity of each fibre type on mesothelial cells at direct contact. Other objective methods to evaluate how easily each fibre reaches the pleural mesothelial cells via a respiratory pathway are mandatory and currently under development.

In conclusion, chrysotile is a strong carcinogen that acts through the induction of local iron overload *in vivo* when it reachs mesothelial cells. Therefore, more appropriate measures have to be taken to reduce environmental cancer risk in this era of human longevity. Since every type of commercially used asbestos causes local 'iron overload' pathology, iron modulation to remove local excess iron [40] might be an encouraging strategy to prevent MM in people who have already been exposed to asbestos. Following the current study, the effects of chrysotile on lung carcinogenesis also require immediate re-evaluation.

Acknowledgment

This study was supported by a MEXT grant (Special Coordination Funds for Promoting Science and Technology); the Princess Takamatsu Cancer Research Fund (10-24213); a Grant-in-Aid for Cancer Research from the Ministry of Health, Labor, and Welfare of Japan; a Grant-in-Aid from the Ministry of Education, Culture, Sports, Science and Technology of Japan; a grant of Long-range Research Initiative by the Japan Chemical Industry Association; and a grant from Takeda Science Foundation.

Abbreviations

aCGH	array-based comparative genomic hybridization
ANOVA	analysis of variance
BAC	bacterial artificial chromosome
BM	biphasic (malignant) mesothelioma
CNT	carbon nanotube
EM	epithelioid (malignant) mesothelioma
FISH	fluorescence *in situ* hybridization
MM	malignant mesothelioma
NTA	nitrilotriacetic acid (nitrilotriacetate)
NTBI	non-transferrin-bound iron
8-OHdG	8-hydroxy-2′-deoxyguanosine
PBS	phosphate-buffered saline
RPMC	rat peritoneal mesothelial cells
SM	sarcomatoid (malignant) mesothelioma
UICC	Unio Internationalis Contra Cancrum

Author contribution statement

LJ and ST conceived and designed the experiments. LJ, SA, HN, HO, SHC, YO, Y. Yoshikawa, KI, and KS performed the experiments. HY, YK, TT, and ST analysed the data. Y. Yamashita, SH, YS, and NK contributed materials. LJ and ST wrote the paper.

References

1. IARC, World Health Organization. Asbestos (chrysotile, amosite, crocidolite, tremolite, actinolite, and anthophyllite). *IARC Monographs on the Evaluation of Carcinogenic Risks to Humans. A Review of Human Carcinogens: Part C: Arsenic, Metals, Fibres, and Dusts*. IARC: Lyon, 2012; 219–309.
2. Roggli VL, Oury TD, Sporn TA (eds). *Pathology of Asbestos-Associated Diseases* (2nd edn). Springer Verlag: New York, 2004.
3. Robinson B, Musk A, Lake R. Malignant mesothelioma. *Lancet* 2005; **366**: 397–408.
4. Robinson B, Lake R. Advances in malignant mesothelioma. *N Engl J Med* 2005; **353**: 1591–1603.
5. Alberg AJ, Ford JG, Samet JM. Epidemiology of lung cancer: ACCP evidence-based clinical practice guidelines (2nd edition). *Chest* 2007; **132**: 29S–55S.
6. Editorials this week: asbestos scandal (16 December 2010). *Nature* 2010; **468**: 868.
7. Smith AH, Wright CC. Chrysotile asbestos is the main cause of pleural mesothelioma. *Am J Ind Med* 1996; **30**: 252–266.
8. 79 Kubota workers killed by asbestos over 26 years. *The Daily Yomiuri*. The Yomiuri Shimbun: Japan; 30 June 2005.
9. Greenberg M. The defence of chrysotile, 1912–2007. *Int J Occup Environ Health* 2008; **14**: 57–66.
10. Hardy JA, Aust AE. Iron in asbestos chemistry and carcinogenicity. *Chem Rev* 1995; **95**: 97–118.
11. Wagner JC, Berry G, Timbrell V. Mesotheliomata in rats after inoculation with asbestos and other materials. *Br J Cancer* 1973; **28**: 173–185.
12. Jiang L, Nagai H, Ohara H, *et al*. Characteristics and modifying factors of asbestos-induced oxidative DNA damage. *Cancer Sci* 2008; **99**: 2142–2151.
13. Nagai H, Okazaki Y, Chew SH, *et al*. Diameter of multi-walled carbon nanotubes is a critical factor in mesothelial injury and subsequent carcinogenesis. *Proc Natl Acad Sci U S A* 2011; **108**: E1330–E1338.
14. Okada S, Hamazaki S, Toyokuni S, *et al*. Induction of mesothelioma by intraperitoneal injections of ferric saccharate in male Wistar rats. *Br J Cancer* 1989; **60**: 708–711.
15. Hu Q, Akatsuka S, Yamashita Y, *et al*. Homozygous deletion of *CDKN2A/2B* is a hallmark of iron-induced high-grade rat mesothelioma. *Lab Invest* 2010; **90**: 360–373.
16. Jiang L, Yamashita Y, Toyokuni S. A novel method for efficient collection of normal mesothelial cells *in vivo*. *J Clin Biochem Nutr* 2010; **46**: 265–268.
17. Toyokuni S, Tanaka T, Hattori Y, *et al*. Quantitative immunohistochemical determination of 8-hydroxy-2′-deoxyguanosine by a monoclonal antibody N45.1: its application to ferric nitrilotriacetate-induced renal carcinogenesis model. *Lab Invest* 1997; **76**: 365–374.
18. Shirase T, Mori K, Okazaki Y, *et al*. Suppression of *SLC11A2* expression is essential to maintain duodenal integrity during dietary iron overload. *Am J Pathol* 2010; **177**: 677–685.
19. Toyokuni S, Kawaguchi W, Akatsuka S, *et al*. Intermittent microwave irradiation facilitates antigen–antibody reaction in western blot analysis. *Pathol Int* 2003; **53**: 259–261.
20. Hagiwara Y, Hamada Y, Kuwahara M, *et al*. Establishment of a novel specific ELISA system for rat N- and C-ERC/mesothelin. Rat ERC/mesothelin in the body fluids of mice bearing mesothelioma. *Cancer Sci* 2008; **99**: 666–670.
21. Sasaki K, Ikuta K, Tanaka H, *et al*. Improved quantification for non-transferrin-bound iron measurement using high-performance liquid chromatography by reducing iron contamination. *Mol Med Rep* 2011; **4**: 913–918.
22. Mottola HA. Nitrilotriacetic acid as a chelating agent: applications, toxicology, and bio-environmental impact. *Toxicol Environ Chem Rev* 1974; **71**: 99–161.
23. Anderson RL, Bishop WE, Campbell RL. A review of the environmental and mammalian toxicology of nitrilotriacetic acid. *Crit Rev Toxicol* 1985; **15**: 1–102.
24. Toyokuni S. Iron-induced carcinogenesis: the role of redox regulation. *Free Radic Biol Med* 1996; **20**: 553–566.
25. Toyokuni S. Role of iron in carcinogenesis: cancer as a ferrotoxic disease. *Cancer Sci* 2009; **100**: 9–16.
26. Toyokuni S, Sagripanti JL. Iron-mediated DNA damage: sensitive detection of DNA strand breakage catalyzed by iron. *J Inorg Biochem* 1992; **47**: 241–248.
27. Toyokuni S, Okada S, Hamazaki S, *et al*. Combined histochemical and biochemical analysis of sex hormone dependence of ferric nitrilotriacetate-induced renal lipid peroxidation in ddY mice. *Cancer Res* 1990; **50**: 5574–5580.
28. Dunn L, Rahmanto Y, Richardson D. Iron uptake and metabolism in the new millennium. *Trends Cell Biol* 2007; **17**: 93–100.
29. Cheng L, Zhou Z, Flesken-Nikitin A, *et al*. Rb inactivation accelerates neoplastic growth and substitutes for recurrent amplification of *cIAP1*, *cIAP2* and *Yap1* in sporadic mammary carcinoma associated with p53 deficiency. *Oncogene* 2010; **29**: 5700–5711.
30. Lin YF, Tsai WP, Liu HG, *et al*. Intracellular beta-tubulin/chaperonin containing TCP1-beta complex serves as a novel chemotherapeutic target against drug-resistant tumors. *Cancer Res* 2009; **69**: 6879–6888.
31. Lee HS, Park MH, Yang SJ, *et al*. Novel candidate targets of Wnt/beta-catenin signaling in hepatoma cells. *Life Sci* 2007; **80**: 690–698.
32. Stanton MF, Layard M, Tegeris A, *et al*. Relation of particle dimension to carcinogenicity in amphibole asbestoses and other fibrous minerals. *J Natl Cancer Inst* 1981; **67**: 965–975.

33. Donaldson K, Aitken R, Tran L, *et al*. Carbon nanotubes: a review of their properties in relation to pulmonary toxicology and workplace safety. *Toxicol Sci* 2006; **92**: 5–22.
34. Husain AN, Colby TV, Ordonez NG, *et al*. Guidelines for pathologic diagnosis of malignant mesothelioma: a consensus statement from the International Mesothelioma Interest Group. *Arch Pathol Lab Med* 2009; **133**: 1317–1331.
35. Shiomi K, Miyamoto H, Segawa T, *et al*. Novel ELISA system for detection of N-ERC/mesothelin in the sera of mesothelioma patients. *Cancer Sci* 2006; **97**: 928–932.
36. Hassan R, Remaley AT, Sampson ML, *et al*. Detection and quantitation of serum mesothelin, a tumor marker for patients with mesothelioma and ovarian cancer. *Clin Cancer Res* 2006; **12**: 447–453.
37. Nagai H, Ishihara T, Lee W-H, *et al*. Asbestos surface provides a niche for oxidative modification. *Cancer Sci* 2012; **102**: 2118–2125.
38. Gazzano E, Turci F, Foresti E, *et al*. Iron-loaded synthetic chrysotile: a new model solid for studying the role of iron in asbestos toxicity. *Chem Res Toxicol* 2007; **20**: 380–387.
39. Toyokuni S. Mysterious link between iron overload and *CDKN2A/2B*. *J Clin Biochem Nutr* 2011; **48**: 46–49.
40. Toyokuni S. Iron as a target of chemoprevention for longevity in humans. *Free Radic Res* 2011; **45**: 906–917.
41. Tanaka T, Iwasa Y, Kondo S, *et al*. High incidence of allelic loss on chromosome 5 and inactivation of $p15^{INK4B}$ and $p16^{INK4A}$ tumor suppressor genes in oxystress-induced renal cell carcinoma of rats. *Oncogene* 1999; **18**: 3793–3797.
42. Xio S, Li D, Vijg J, *et al*. Codeletion of *p15* and *p16* in primary malignant mesothelioma. *Oncogene* 1995; **11**: 511–515.
43. Sekido Y. Inactivation of Merlin in malignant mesothelioma cells and the Hippo signaling cascade dysregulation. *Pathol Int* 2011; **61**: 331–344.
44. Jean D, Thomas E, Manie E, *et al*. Syntenic relationships between genomic profiles of fiber-induced murine and human malignant mesothelioma. *Am J Pathol* 2011; **178**: 881–894.
45. Foster SA, Wong DJ, Barrett MT, *et al*. Inactivation of p16 in human mammary epithelial cells by CpG island methylation. *Mol Cell Biol* 1998; **18**: 1793–1801.
46. Miceli MH, Dong L, Grazziutti ML, *et al*. Iron overload is a major risk factor for severe infection after autologous stem cell transplantation: a study of 367 myeloma patients. *Bone Marrow Transpl* 2006; **37**: 857–864.
47. Miyama K, Yamada G, Yamamoto T, *et al*. A BMP-inducible gene, *dlx5*, regulates osteoblast differentiation and mesoderm induction. *Dev Biol* 1999; **208**: 123–133.
48. Firulli A, McFadden D, Lin Q, *et al*. Heart and extra-embryonic mesodermal defects in mouse embryos lacking the bHLH transcription factor Hand1. *Nature Genet* 1998; **18**: 266–270.
49. Khoo M, McQuade L, Smith M, *et al*. Growth and differentiation of embryoid bodies derived from human embryonic stem cells: effect of glucose and basic fibroblast growth factor. *Biol Reprod* 2005; **73**: 1147–1156.

SUPPORTING INFORMATION ON THE INTERNET

The following supporting information may be found in the online version of this article.

Figure S1. Survival fraction regarding asbestos type, histological type, and NTA administration.

Figure S2. Immunohistochemistry of DMT1.

Figure S3. Expression analysis of asbestos-induced rat MMs.

Figure S4. Analysis of array-based comparative genomic hybridization from the viewpoint of each chromosome and asbestos type.

Figure S5. Analysis of array-based comparative genomic hybridization from the viewpoint of histology.

Table S1. Incidence of asbestos-induced malignant mesothelioma.

Table S2. Primers used for quantitative real-time PCR analysis.

TGF-β synergizes with defects in the Hippo pathway to stimulate human malignant mesothelioma growth

Makiko Fujii,[1] Takeshi Toyoda,[5] Hayao Nakanishi,[2] Yasushi Yatabe,[3] Ayuko Sato,[6] Yasue Matsudaira,[1] Hidemi Ito,[1] Hideki Murakami,[1] Yutaka Kondo,[1] Eisaku Kondo,[2] Toyoaki Hida,[4] Tohru Tsujimura,[6] Hirotaka Osada,[1,7] and Yoshitaka Sekido[1,7]

[1]Division of Molecular Oncology and [2]Division of Oncological Pathology, Aichi Cancer Center Research Institute; and [3]Department of Pathology and Molecular Diagnostics and [4]Department of Thoracic Oncology, Aichi Cancer Center Hospital; Aichi Cancer Center, Chikusa-ku, Nagoya 464-8681, Japan
[5]Division of Pathology, National Institute of Health Sciences, Setagaya-ku, Tokyo 158-8501, Japan
[6]Department of Pathology, Hyogo College of Medicine, Nishinomiya, Hyogo 663-8501, Japan
[7]Department of Cancer Genetics, Program in Function Construction Medicine, Nagoya University Graduate School of Medicine, Showa-ku, Nagoya 466-8550, Japan

Malignant mesothelioma (MM) is an incurable malignancy that is caused by exposure to asbestos and is accompanied by severe fibrosis. Because MM is usually diagnosed at an advanced stage and clinical identification of early lesions is difficult, its molecular pathogenesis has not been completely elucidated. Nearly 75% of MM cases have inactivating mutations in the *NF2* (*neurofibromatosis type 2*; Merlin) gene or in downstream signaling molecules of the Hippo signaling cascade, which negatively regulates the transcription factor Yes-associated protein (YAP). In this study, we demonstrate a functional interaction between the Hippo and TGF-β pathways in regulating connective tissue growth factor (CTGF). Expression of CTGF in MM cells was induced by the formation of a YAP–TEAD4–Smad3–p300 complex on the *CTGF* promoter. Knocking down CTGF expression in MM cells prolonged the survival of xenografted mice, and a significant association was seen between CTGF expression and extracellular matrix deposition in MM xenografts and in patient tissue specimens. We further suggest that CTGF may influence the malignancy of mesothelioma because of the different histological expression patterns observed in human MM tissues. These data suggest that CTGF is an important modulator of MM growth and pathology and represents a novel therapeutic target for this disease.

CORRESPONDENCE
Makiko Fujii:
fujiim@aichi-cc.jp
OR
Yoshitaka Sekido:
ysekido@aichi-cc.jp

Abbreviation used: CC, coiled-coil; ChIP, chromatin immunoprecipitation; CTGF, connective tissue growth factor; ECM, extracellular matrix; MM, malignant mesothelioma; mRNA, messenger RNA; shRNA, short hairpin RNA; TEAD, TEA domain family member; YAP, Yes-associated protein.

Malignant mesothelioma (MM), arising from serosal cells of the pleural, peritoneal, and pericardial cavities, has a poor prognosis because it is frequently diagnosed at advanced stages. The primary cause of this disease has often been linked to asbestos exposure, and the number of patients worldwide is predicted to peak in the next two decades (Robinson and Lake, 2005; Murayama et al., 2006). The latent period between first exposure to asbestos and onset of the disease is ~20–40 yr, and the first symptom is insidious and may include chest pain and breathlessness. Although there has been significant recent progress in clinical treatment with combination chemotherapies, a curative therapy for MM is still unknown, with the median survival ranging between 9 and 17 mo from the first diagnosis (Tsao et al., 2009).

The involvement of tumor suppressor genes, including $p16^{INK4a}/p14^{ARF}$ and *NF2* (*neurofibromatosis type 2*), has been demonstrated to be crucial in the development of various MMs (Bianchi et al., 1995; Sekido et al., 1995). The *NF2* gene, known to be responsible for NF2 syndrome, encodes Merlin, and deletions or mutations of this gene were found in 40–50% of MMs. The downstream signaling of Merlin is the mammalian Hippo cascade, which was originally identified by genetic studies in *Drosophila melanogaster* (Hay and Guo, 2003; Ryoo and Steller, 2003; Wu et al., 2003;

The Rockefeller University Press $30.00
J. Exp. Med. Vol. 209 No. 3 479-494
www.jem.org/cgi/doi/10.1084/jem.20111653

Hamaratoglu et al., 2006). The Hippo signaling cascade is a critical regulator of organ size in *Drosophila* as well as in mammals (Dong et al., 2007). In the conditional transgenic mouse model, the dysregulation of the pathway leads to tumorigenesis (Zhang et al., 2010). Considering Merlin and downstream components of the Hippo cascade, SAV1 (Salvador 1) and LATS2 (large tumor suppressor 2), 75% of MM cell lines had genetic inactivation of at least one of these three proteins (Murakami et al., 2011). Merlin inhibits the transcriptional coactivation activity of Yes-associated protein (YAP) by inducing phosphorylation and cytoplasmic retention of YAP (Yokoyama et al., 2008). YAP accumulation in the nucleus is also observed in MMs accompanied by mutation or deletion of *LATS2* (Murakami et al., 2011). YAP is a possible oncogene that associates with TEAD (TEA domain family member), a transcription factor, and exerts biological functions such as gene expression stimulation, cell growth, anchorage-independent cell growth, and epithelial-mesenchymal transition (Vassilev et al., 2001; Zhao et al., 2008, 2009).

TGF-β was originally identified as a protein that mediates the transformation of nonneoplastic rat kidney and murine AKR-2B fibroblasts (de Larco and Todaro, 1978; Moses et al., 1981; Anzano et al., 1983). TGF-β can induce extremely variable responses depending on the cell type, mainly through the Smad2/3-dependent pathway. For example, TGF-β induces growth arrest and apoptosis in epithelial cells; it can also activate fibroblasts. Subsequent studies further revealed that TGF-β acts as a tumor suppressor in premalignant cells as well as cells progressing through the early stages of carcinogenesis; furthermore, it exerts prooncogenic effects in metastatic tumors (Roberts and Wakefield, 2003; Massagué, 2008). TGF-β is a powerful cytokine produced by many different cell types, with effects on multiple cell types, and because of this complexity, signaling in each cell and context should be carefully studied.

Upon TGF-β stimulation, Smad2 and Smad3 form complexes with Smad4 and accumulate in the nucleus (Massagué et al., 2005). p300, a transcriptional co-activator, binds with Smad3 and Smad2 and enhances Smad-induced transactivation of target genes (Nishihara et al., 1998). Recruitment of p300 frequently plays a core role not only in enhancing transactivation but also in binding other proteins to stabilize protein complexes (Fujii et al., 2006).

Mesothelial cells were reported to demonstrate an increase in DNA synthesis after TGF-β stimulation (Gabrielson et al., 1988), and both normal human mesothelial cells and MM cell lines secrete TGF-β (Gerwin et al., 1987). Furthermore, a soluble TGF-β type II receptor inhibitor and a TGF-β type I receptor kinase inhibitor (SM16) were shown to inhibit the growth of murine MM tumors injected into the flanks of mice through the reactivation of antitumor immune responses (Suzuki et al., 2004, 2007).

Given the involvement of genetic inactivation of components of the Hippo pathway in 75% of mesotheliomas and previous evidence for a protumorigenic role for the TGF-β pathway, we examined the relationship between these two pathways to further understand the molecular mechanisms underlying mesothelioma genesis. Cross talk between the Hippo and TGF-β and BMP (bone morphogenetic protein) signaling pathways has been previously reported (Varelas et al., 2008, 2010; Alarcón et al., 2009). TAZ controls nucleocytoplasmic localization of Smad2/3–Smad4 complexes and regulates the nuclear accumulation of Smad complexes (Varelas et al., 2008). Furthermore, TAZ and YAP dictate the localization of active Smad complexes during mouse embryogenesis (Varelas et al., 2010). YAP is also known to strongly bind to Smad1 and support Smad1-dependent transcription and is required for BMP suppression of neural differentiation in mouse embryonic stem cells (Alarcón et al., 2009). However, whether the cross talk between Hippo and TGF-β signaling plays an important role in tumorigenesis has not been elucidated. We found that YAP and Smad3 interact at the transcription regulation level through participants of other related transcription cofactors, forming a complex in the *connective tissue growth factor* (*CTGF*) promoter region and thereby enhancing CTGF expression. This evidence shows that the cross talk between the Hippo and TGF-β pathway directly controls prooncogenic effects in malignancy. We further show that antagonism of the TGF-β pathway and CTGF expression can prolong the survival of mice with MM tumor xenografts, suggesting new approaches for the treatment of MM.

RESULTS

The TGF-β–Smad pathway is activated in clinical samples of human mesothelioma and regulates proliferation and extracellular matrix (ECM) production in MM cells in vitro

To assess the involvement of the TGF-β pathway in MM tumor growth, we performed immunohistochemical analysis in 24 tissue specimens obtained from patients to determine the p-Smad2 level and evaluate whether MM cells receive TGF-β signaling during their growth. In all 24 samples, which were subtyped into three major categories, epithelioid (12 patients), biphasic (3 patients), and sarcomatoid (7 patients), p-Smad2 staining was strongly observed in nuclei. This suggested that the constitutive activation of TGF-β is important for MM tumor development (Fig. 1 A and see Table 2). Histological subtype is a significant prognostic factor associated with longer survival because the median survival for patients with epithelioid tumors is 16.3 mo, which is longer than that for patients with biphasic tumors (9.5 mo) and sarcomatoid tumors (6.1 mo; Flores et al., 2007). Samples from all three subtypes exhibited the same level of p-Smad2 nuclear staining, indicating that the activation of the TGF-β pathway is maintained across different grades of malignancies, whereas normal pleural mesothelial cells did not exhibit significant p-Smad2 signals (Fig. 1 B, top, arrowheads). Interestingly, the nuclei of reactive pleural mesothelial cells, which were adjacent to the mesothelioma, having cuboidal appearance may be under serosal stimulation and were positively stained by p-Smad2, suggesting that the surrounding tissues were also affected by paracrine TGF-β signaling (Fig. 1 B, bottom).

TGF-β promotes proliferation and ECM production in normal and malignant mesothelial cells

To examine whether TGF-β signaling affects monolayer cell growth, we compared cell growth by counting cell number after exposing cells to a TGF-β type I receptor kinase inhibitor, SD-208. MeT-5A is a nonmalignant human pleural mesothelial cell line immortalized by SV40 early region DNA (Ke et al., 1989). Phosphorylation of Smad3 by TGF-β peaked around 1 h and gradually decreased later in the MeT-5A cells and MM cell lines (Fig. S1 A). The proliferation and the activation of MeT-5A cells and MM cell lines, as well as the Smad-dependent pathway induced by TGF-β in these cells were effectively suppressed by TGF-β type I receptor kinase inhibitor (Fig. 1 C and Fig. S1, B and C). To further assess

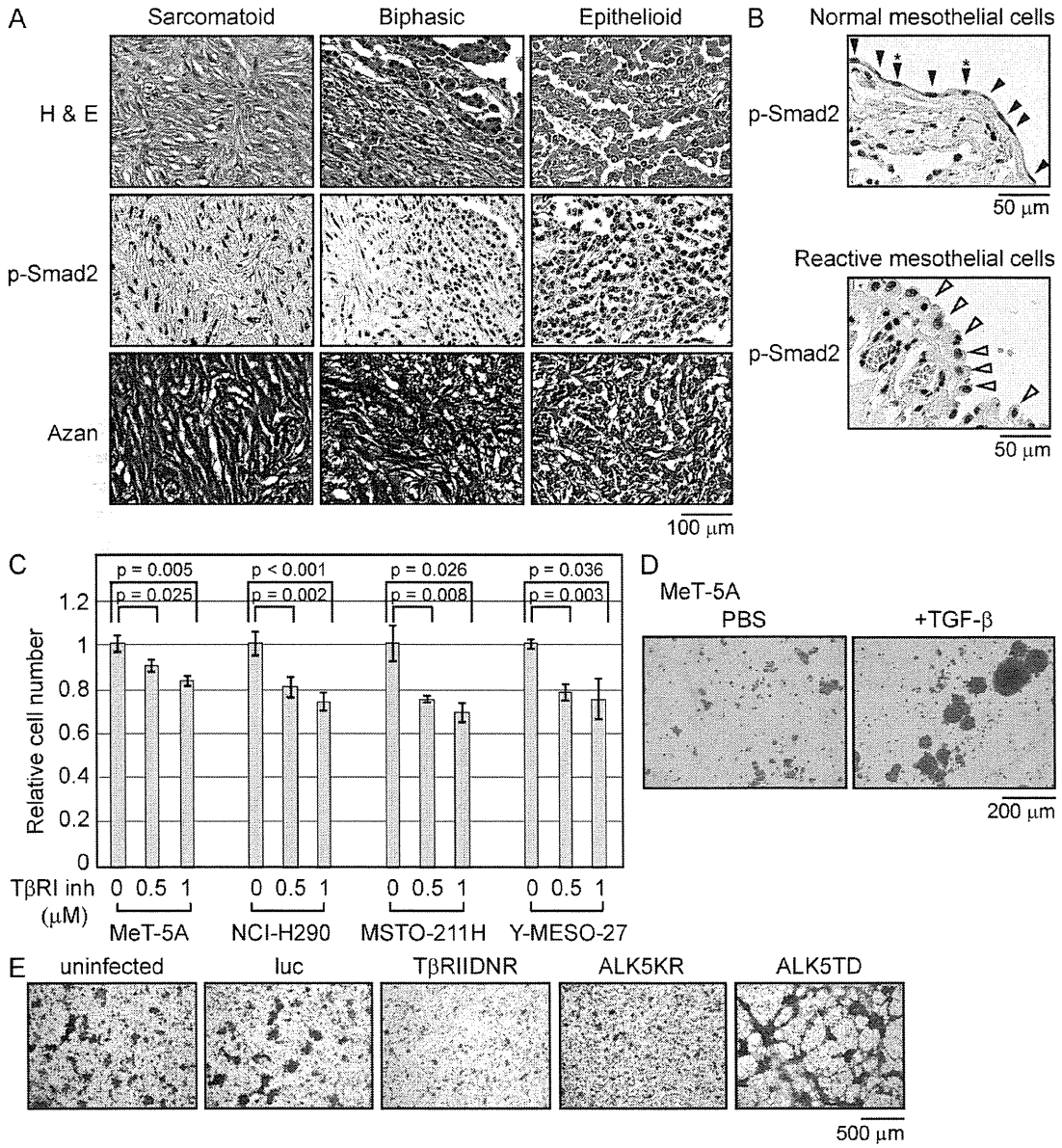

Figure 1. TGF-β signaling affects the growth of human MM cells. (A) Immunohistochemical staining for p-Smad2 of MM tissues derived from patients. Three representative sections, namely sarcomatoid, biphasic, and epithelioid subtype tumors, are shown. Azan staining was performed to visualize collagen fibers. H&E, hematoxylin and eosin. (B) Immunohistochemical staining for p-Smad2 in normal mesothelial cells (closed arrowheads) from normal lungs and reactivated normal mesothelial cells (open arrowheads) adjacent to MM tumors. Asterisks show cells with positive nuclear staining in normal mesothelial cells. (C) Cell numbers were counted 3 d after treatment with TGF-β type I receptor kinase inhibitor (SD-208). Results are expressed as mean ± SEM and are representative of three independent assays. (D) Soft agar colony formation assay was performed using MeT-5A cells treated with 4 ng/ml TGF-β for 7 d. The panel is representative of three independent assays. (E) NCI-H290 cells were infected with the indicated lentiviral expression vectors and stained with Giemsa after 14 d. HA-tagged luciferase (luc) was used as a control. The panel is representative of three independent assays. TβRIIDNR, dominant-negative form of the TGF-β type II receptor; ALK5KR, dominant-negative form of the TGF-β type I receptor; ALK5TD, constitutively activated TGF-β type I receptor.

Table 1. Common genes responsive to TGF-β in MeT-5A and Y-MESO-27 cells

Symbol	Description
MeT-5A and Y-MESO-27 common genes up (>1.5fold)	
CSF1R	colony-stimulating factor 1 receptor
SNAI1	snail homologue 1
*LOX**	lysyl oxidase
RASGRP1	RAS guanyl-releasing protein 1
*MMP2**	matrix metallopeptidase 2
*ITGA11**	integrin, alpha 11
SERPINE1	plasminogen activator inhibitor type 1
BMP6	bone morphogenetic protein 6
GDF6	growth differentiation factor 6
*COL1A1**	Prepro-alpha1(I) collagen
EDN1	endothelin 1
*COL1A2**	collagen, type I, alpha 2
MFAP4	microfibrillar-associated protein 4
SERPINE2	plasminogen activator inhibitor type 1, member 2
*COL20A1**	collagen, type XX, alpha 1
*COL5A1**	collagen, type V, alpha 1
*ITGB3**	integrin, beta 3
LTBP2	latent transforming growth factor beta binding protein 2
SMAD7	SMAD family member 7
*COL7A1**	collagen, type VII, alpha 1
SKIL	SKI-like oncogene
*COL4A1**	collagen, type IV, alpha 1
TGFB1	transforming growth factor, beta 1
*ITGAV**	integrin, alpha V (vitronectin receptor)
IGFBP3	insulin-like growth factor binding protein 3
*COL4A4**	collagen, type IV, alpha 4
CDH11	cadherin 11, type 2, OB-cadherin (osteoblast)
GADD45B	growth arrest and DNA-damage-inducible, beta
ADAM12	ADAM metallopeptidase domain 12
BMPR2	bone morphogenetic protein receptor, type II
*ITGA1**	integrin, alpha 1
*COL16A1**	collagen, type XVI, alpha 1
MDAC1	MDAC1
TGFB2	transforming growth factor, beta 2
EGR2	early growth response 2
*CTGF**	connective tissue growth factor
ID3	inhibitor of DNA binding 3
*FN1**	fibronectin
MeT-5A and Y-MESO-27 common genes down (<0.67-fold)	
IL6R	interleukin 6 receptor
VCAM1	vascular cell adhesion molecule 1
CASP1	caspase 1, apoptosis-related cysteine peptidase
IL12A	interleukin 12, alpha
IL1A	interleukin 1, alpha
IL7	interleukin 7
FAS	TNF receptor superfamily, member 6
*MMP26**	matrix metallopeptidase 26
FGF23	fibroblast growth factor 23
CAMK2A	calcium/calmodulin-dependent protein kinase II alpha
NEDD4L	neural precursor cell expressed, developmentally down regulated 4-like
*COL24A1**	collagen, type XXIV, alpha 1
TGFA	transforming growth factor, alpha
CAMK2D	calcium/calmodulin-dependent protein kinase II delta
TLR3	toll-like receptor 3
BCL2	B-cell CLL/lymphoma 2

MeT-5A and Y-MESO-27 cells were treated with TGF-β for 24 h. Total RNA was extracted and subjected to microarray analysis. The genes encoding ECM-related protein are indicated by an asterisk.

the biological activity of TGF-β in mesothelial cells, we performed an anchorage-independent cell proliferation assay with MeT-5A cells. After 7 d, colony formation was observed, showing the innate response of MeT-5A cells to TGF-β, which promotes colony formation similarly to that observed in fibroblasts (Fig. 1 D). Using a lentiviral vector system, we examined whether TGF-β signaling could modulate focus formation in NCI-H290 cells, an MM cell line (Fig. 1 E). Examination of the foci formed after 14 d showed a prominent decrease in the number of foci formed in cells expressing dominant-negative forms of the TGF-β type I and type II receptors. Conversely, cells with constitutive activation of the TGF-β type I receptor showed aggressive formation of foci, suggesting that TGF-β signaling affects the oncogenic property of mesothelioma cells.

To further investigate the molecular consequences of TGF-β pathway activation in mesothelioma cells, we performed cDNA microarray analysis to elucidate alterations in gene expression profiles after TGF-β treatment in MeT-5A and Y-MESO-27 cells (Table 1). Looking for overlap in the gene expression profiles, we found that 54 genes were regulated more than 1.5-fold by TGF-β in both cell types after 24 h of treatment. 42% of the commonly up-regulated genes (16/38) in TGF-β–treated MeT-5A cells and Y-MESO-27 cells were classified as ECM-related proteins. Changes in the expression profiles of representative genes (e.g., *MMP2*, *CTGF*, *COL1A1*, and *TGF-β*) were confirmed by real-time RT-PCR (Fig. S1, D and E).

YAP is critical for TGF-β induction of a small number of target genes

Genetic alteration of the tumor suppressor gene *NF2* and downstream components of the Hippo pathway, *SAV1* and *LATS2*, were observed in 75% of MM tumors (Murakami et al., 2011). This suggests that the disturbance of the Hippo pathway is strongly associated with the development of mesothelioma. Merlin, a protein encoded by *NF2*, *SAV1*, or *LATS*, negatively regulates YAP, whose oncogenic property has been recently reported (Wang et al., 2009). Dephosphorylated YAP translocates into the nucleus, where it binds to TEAD and activates the transcription of target genes. Merlin inhibits the

transcriptional coactivation activity of YAP by inducing phosphorylation and cytoplasmic retention of YAP (Yokoyama et al., 2008). Furthermore, genome-wide comprehensive genomic hybridization analysis of 22 MM specimens from patients showed that there is high copy amplification of 11q22 regions containing the *YAP* oncogene (Taniguchi et al., 2007). Thus, many genetic alterations in the Hippo pathway that have been seen in mesothelioma converge to increase YAP activity.

To analyze the possible alteration in TGF-β response in mesothelioma cells caused by defects in the Hippo pathway, we suppressed endogenous YAP expression using short hairpin RNA (shRNA) vectors in NCI-H290 cells, which have a genetic deletion of *NF2*. *YAP* messenger RNA (mRNA) expression was successfully down-regulated in shYAP-transfected cells without any alteration after treatment of TGF-β for either 2 or 24 h. *YAP* expression was not affected by TGF-β treatment in MM cells (Fig. 2 A). Because YAP is a known transcriptional modulator, we investigated the effect of *YAP* down-regulation on mRNA levels of genes regulated by TGF-β. Interestingly, genes regulated by TGF-β could be categorized into one of three groups. The expression of *fibronectin* and *COL1A1* did not immediately change; however, these genes were later activated by TGF-β, suggesting that they may be the target of a secondary response to TGF-β.

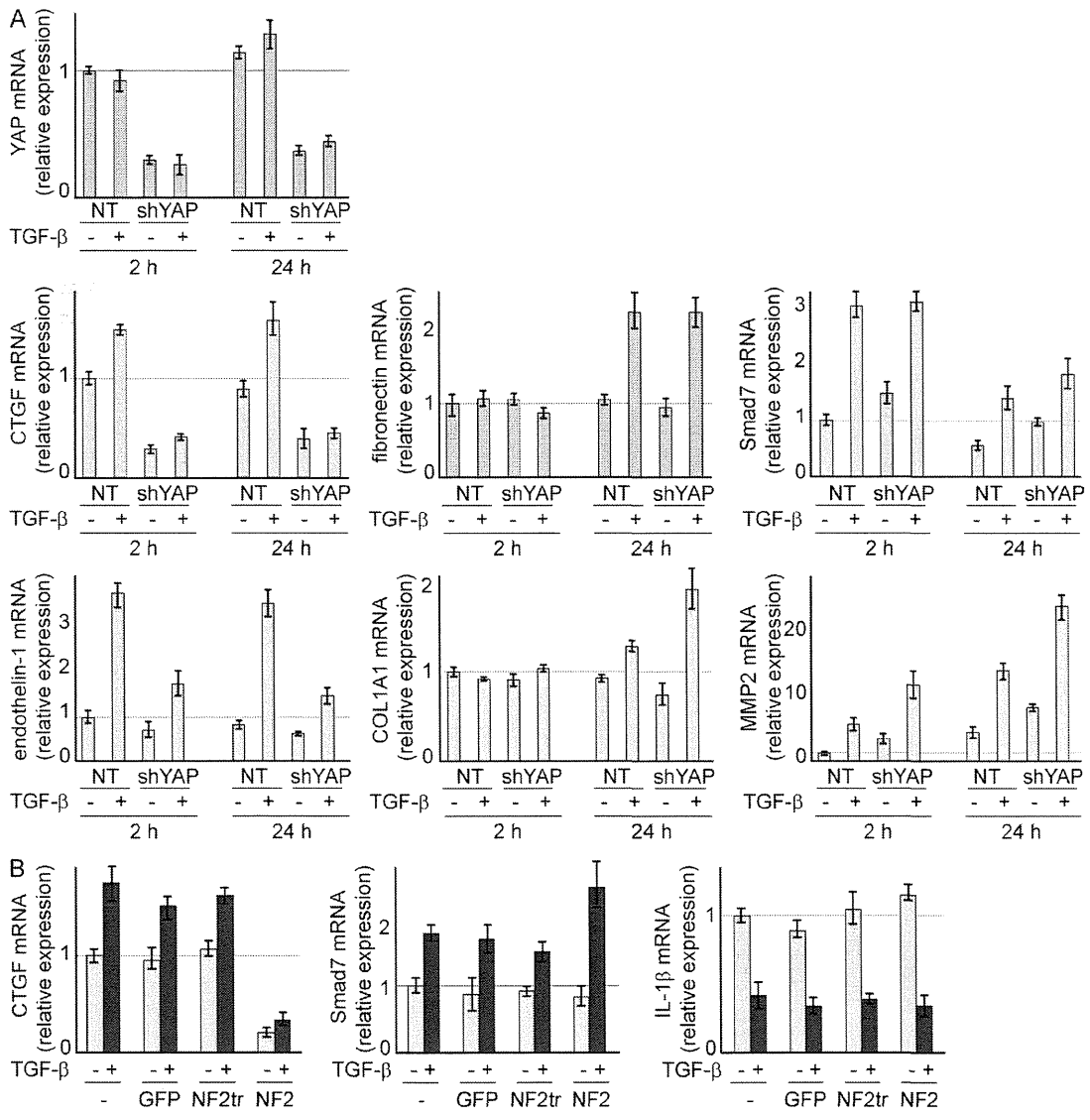

Figure 2. The CTGF expression level was modulated by the TGF-β and Hippo pathways in MM cells. (A) NCI-H290 cells, which show homologous deletion of *NF2* with concomitant YAP translocation to the nucleus, were transfected with plasmids containing shYAP. After 48 h of puromycin selection, TGF-β was added, followed by mRNA extraction after 2 and 24 h to perform real-time RT-PCR to evaluate gene expression. A plasmid with a nontarget sequence (NT) was used as the control. (B) Lentiviral vectors containing full-length and truncated NF2 that lack the ability to phosphorylate YAP on Ser 127 were used to infect NCI-H290 cells. Real-time RT-PCR was performed using mRNA extracted 2 h after TGF-β treatment. −, untreated or uninfected; NF2tr, truncated NF2. (A and B) Results are expressed as mean ± SEM and are representative of three independent assays.

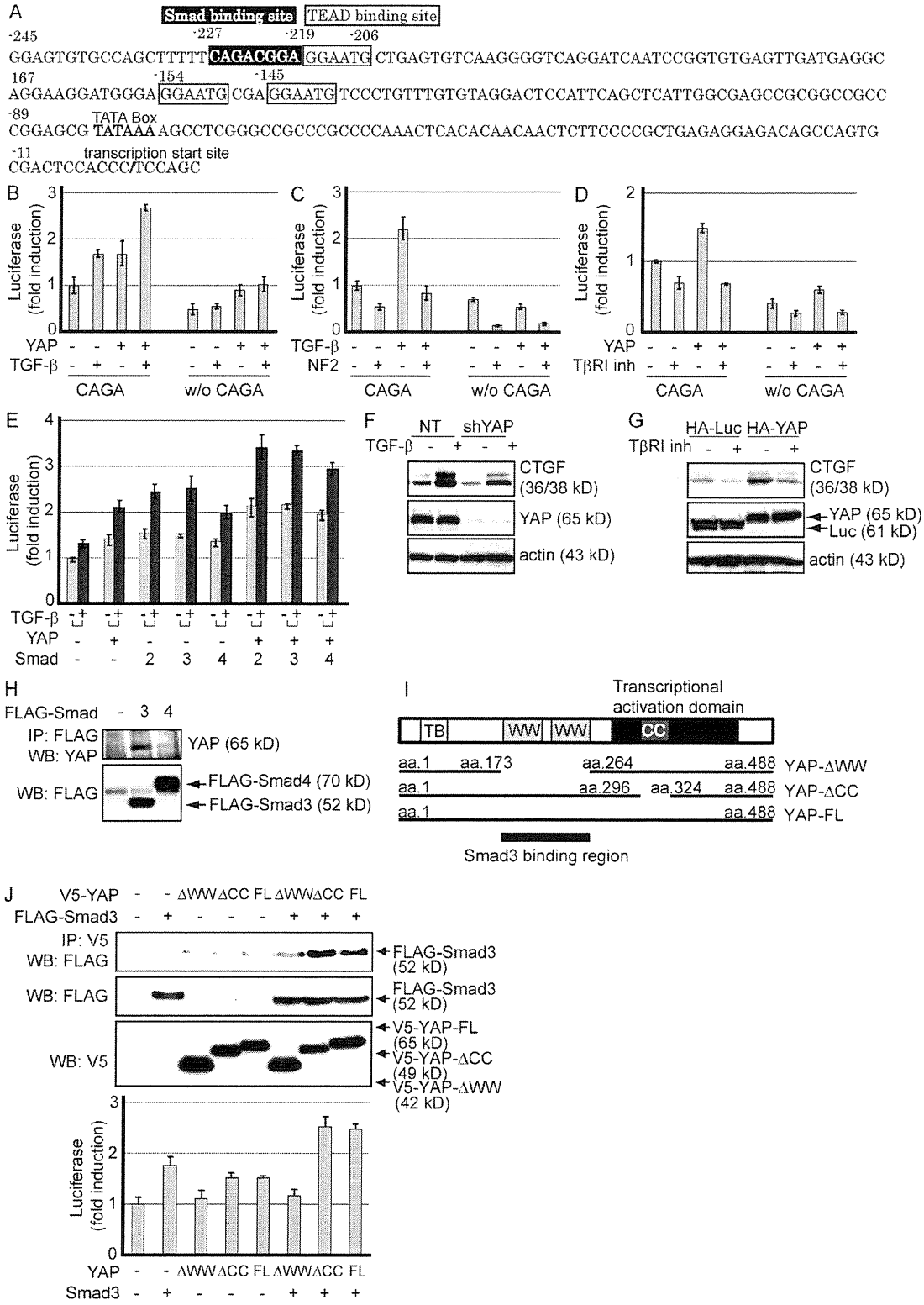

Figure 3. Smad3 interacts with YAP and enhances the transactivation activity of the *CTGF* promoter. (A) The human *CTGF* promoter region contains a Smad-binding site (−227 to −220) and a TEAD-binding site (−219 to −214) adjacent to each other. A luciferase reporter plasmid was linked to the *CTGF* promoter with (*CAGA*, −245 to 16) or without (w/o *CAGA*, −206 to 16) the Smad/TEAD-binding sites indicated. (B–D) NCI-H290 cells were transfected with *CTGF*-luciferase reporter plasmids with or without the Smad/TEAD-binding sites, together with the indicated plasmids. After 24 h, either the TGF-β or TβRI inhibitor was added to

Smad7 and *MMP2* were up-regulated by TGF-β within 2 h, but *YAP* depletion did not affect this activation. *CTGF* and *endothelin-1* were activated by TGF-β within 2 h, and this activation was suppressed by knockdown of endogenous *YAP*. Surprisingly, the number of functionally known genes identified by expression microarray, up-regulated in control versus TGF-β by >1.5-fold and also down-regulated in nontarget shRNA with TGF-β versus shYAP with TGF-β by <0.67-fold, was limited to these two genes in NCI-H290 cells (unpublished data). The aforementioned observations suggest that *YAP* does not influence the expression of all TGF-β target genes but does affect the transactivation of select genes. To confirm this result, NCI-H290 cells were infected with lentivirus vector carrying *GFP*, full-length *NF2*, or *NF2* with the truncated FERM (four-point-one/ezrin/radixin/moesin) domain. FERM truncation resulted in loss in the ability to phosphorylate YAP on Ser 127 (Yokoyama et al., 2008). Although neither *Smad7* up-regulation nor *IL-1β* down-regulation was affected, irrespective of TGF-β treatment, *CTGF* was greatly suppressed by *NF2* overexpression (Fig. 2 B).

YAP associates with Smad2/3 and synergistically enhances the transactivation of CTGF

TGF-β is known to positively regulate CTGF expression through Smad activation in NIH 3T3 fibroblasts (Holmes et al., 2001) and induces fibrosis in vivo. YAP binds to TEAD, and it is recruited to the putative TEAD-binding site that resides on the *CTGF* promoter (Zhao et al., 2008). We found that the *CTGF* promoter contains both a TEAD-binding site and a consensus Smad-binding site adjacent to each other (Fig. 3 A). Smad3 is a crucial mediator of TGF-β signaling, directly activating genes through Smad3/Smad4 DNA-binding motifs in mouse embryo fibroblasts (Yang et al., 2003; Roberts et al., 2006). To examine whether the TGF-β pathway and YAP may regulate the transcriptional activity of *CTGF*, we generated *CTGF* promoters containing or lacking this Smad/TEAD-binding site linked to luciferase. Treatment with TGF-β as well as overexpression of YAP enhanced the transcriptional activity of the *CTGF* promoter with the Smad-binding site in NCI-H290 cells. Deletion of the Smad/TEAD-binding site weakened basal promoter activities and responses to YAP (Fig. 3 B). The slight induction by TGF-β was possibly through TEAD-binding sites and might be the effects of the complex formation described in Fig. 4. Merlin, a protein encoded by *NF2*, suppresses TGF-β–induced activation, indicating the involvement of the Hippo signaling pathway in *CTGF* promoter activation by TGF-β (Fig. 3 C). On the contrary, TGF-β type I receptor kinase inhibitor blocked the transactivation by YAP (Fig. 3 D). Transfection of vectors carrying Smad2, Smad3, and Smad4 together with YAP enhanced the transcriptional activity of the *CTGF* promoter, which was further activated by TGF-β treatment (Fig. 3 E). The data suggest that Smad3 and YAP can synergize to up-regulate CTGF expression.

To confirm these results at the protein level, we overexpressed YAP in MM cells and investigated whether CTGF protein expression was modulated by the TGF-β pathway and YAP. Depletion of endogenous YAP suppressed CTGF protein expression in both cell lines, irrespective of TGF-β treatment (Fig. 3 F). Conversely, TGF-β type I receptor kinase inhibitor suppressed YAP-enhanced CTGF expression (Fig. 3 G). These results further support the possible involvement of two distinct pathways in CTGF regulation.

Functional and physical associations between Smads and WW domain–containing proteins such as TAZ and YAP have been demonstrated, and these associations were implicated in the transcription of multiple target genes (Varelas et al., 2008; Alarcón et al., 2009). We found that YAP binds to Smad3 but not to Smad4 (Fig. 3 H). To identify the requisite domain in the Smad3–YAP interaction, we used YAP deletion constructs, which lacked either WW or coiled-coil (CC) domains (Fig. 3 I). Smad3 could be coimmunoprecipitated with YAP-ΔCC, but a prominent decrease in binding was observed with YAP-ΔWW, suggesting that the WW domain is important for YAP binding to Smad3 (Fig. 3 J, top). In agreement with this result, although YAP-ΔCC could enhance the transcriptional activity of the *CTGF* promoter, YAP-ΔWW failed to augment this activity (Fig. 3 J, bottom). These data suggest the functional interaction through the YAP-WW domain with Smad3 in regulating CTGF expression.

YAP, Smad3, TEAD, and p300 comprise a common complex

Although the aforementioned results suggest physical binding and functional interactions between YAP and Smad3, the affinity of these proteins are not strong compared with the interaction of YAP with Smad1, as previously shown in HEK293T cells (Alarcón et al., 2009). To address this issue, we assessed the possible involvement of components in complex

the medium and incubated for an additional 24 h. Fold induction of transcriptional response relative to untreated cells is shown. Results are expressed as mean ± SEM and are representative of three independent assays. (E) Effects of TGF-β treatment on the activation of the *CTGF* promoter by YAP and Smads in NCI-H290 cells. Fold induction of transcriptional response relative to untreated cells is shown. Results are expressed as mean ± SEM and are representative of three independent assays. (F) Y-MESO-27 cells were lentivirally infected with either nontarget (NT) or YAP shRNA (shYAP) vector, followed by treatment with TGF-β type I receptor kinase inhibitor. Protein levels were determined by Western blotting. (G) Y-MESO-27 cells were lentivirally infected to express YAP protein and were treated with TGF-β. A lentivirus vector containing HA-luciferase was used as a control. Protein levels were determined by Western blotting. (H) HEK293 cells were transiently transfected with flag-tagged Smad vectors, and lysates were subjected to immunoprecipitation (IP), followed by Western blotting (WB) with anti-YAP antibody. Expression levels of exogenous Smads were confirmed in the bottom panel. (I) Schematic representation of the deletion constructs of YAP. CC, CC domains; FL, full length; TB, TEAD-binding domain; WW, WW domains. (J) HEK293 cells were transiently transfected with the indicated plasmids and subjected to immunoprecipitation. Western blotting was performed to confirm the expression level of YAP and Smad3 (top). NCI-H290 cells were transfected with the *CTGF*-luciferase reporter plasmid and combinations of Smad3 and YAP deletion constructs (bottom). Results are mean ± SEM and are representative of three independent assays.

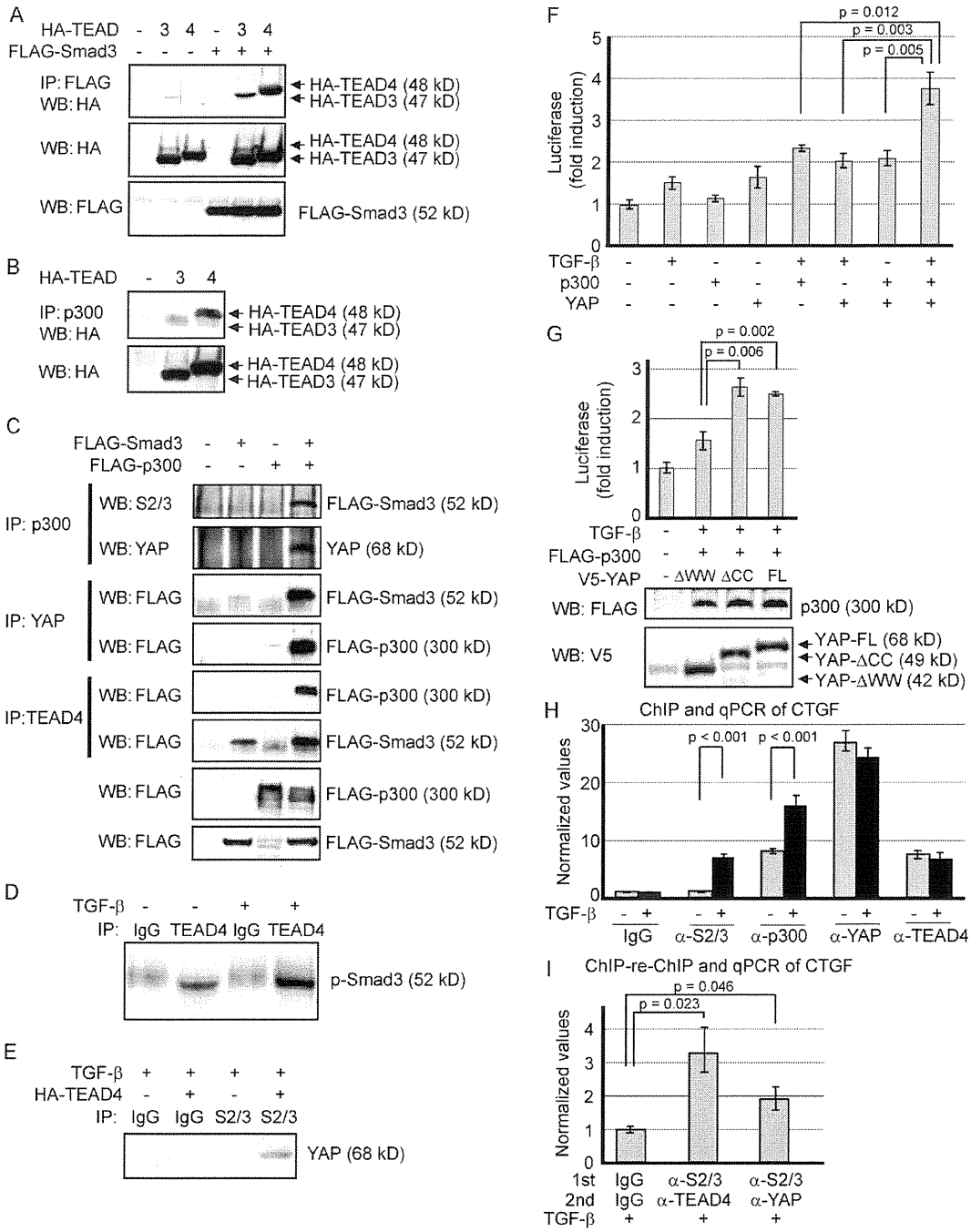

Figure 4. Smad3, YAP, TEAD, and p300 are components of a functional complex on the *CTGF* promoter. (A and B) HEK293 cells were transiently co-transfected with indicated plasmids, and lysates were subjected to immunoprecipitation (IP) followed by Western blotting (WB). (C) HEK293 cells were transfected with expression vectors as indicated. Cell lysates were divided and subjected to immunoprecipitation using p300, YAP, and TEAD4 antibodies. Samples subjected to Western blot are shown in the lowest panels. (D) Interaction between endogenous TEAD4 and p-Smad3 was examined using TGF-β–treated Y-MESO-27 cells. (E) Y-MESO-27 cells were infected with a TEAD4 lentiviral vector. After 4 d, the cells were treated with TGF-β, and lysates were immunoprecipitated with Smad2/3 antibodies and detected by YAP antibodies. (F) NCI-H290 cells were transfected with the *CTGF*-luciferase reporter plasmid and combinations of TGF-β, YAP, and p300. Results are expressed as mean ± SEM and are representative of three independent assays. (G) NCI-H290 cells were transfected with the *CTGF*-luciferase reporter together with the indicated plasmids. Luciferase activity (top) and protein levels (bottom) are shown. Results are expressed as mean ± SEM and are representative of three independent assays. (H) ChIP analysis was performed using MSTO-211H cells by pulling down endogenous Smad2/3, p300, YAP, and TEAD4. *CTGF* promoter with Smad- and TEAD-binding adjacent regions was amplified by PCR. The value was normalized by input. The results shown are representative of three independent assays. (I) ChIP-reChIP assay was performed using TGF-β–treated MSTO-211H cell lysates, followed by quantitative PCR (qPCR). The first and second primary antibodies used for immunoprecipitation are indicated. (H and I) Results are expressed as mean ± SEM and are representative of three independent assays.

formation to further demonstrate both binding and functional activity.

Transient transfection experiments with HEK293 cells revealed that Smad3, p300, and YAP coprecipitate with both TEAD3 and TEAD4, although binding affinity was much stronger for TEAD4, compared with TEAD3 (Fig. 4, A and B). An immunoprecipitation assay using HEK293T cells with ectopic expression of Smad3 and p300 showed that the binding between ectopic p300 and endogenous YAP was enhanced in the presence of ectopic Smad3 (Fig. 4 C, second panel). The interaction of endogenous YAP with ectopic Smad3 was enhanced in the presence of ectopic p300 (Fig. 4 C, third panel), and on the contrary, the binding of ectopic p300 to endogenous YAP was much stronger in the presence of Smad3 (Fig. 4 C, fourth panel). Furthermore, endogenous TEAD4 bound to ectopic p300 in the presence of ectopic Smad3 and with ectopic Smad3 in the presence of ectopic p300 (Fig. 4 C, fifth and sixth panels). Using Y-MESO-27 cells, an MM cell line in which *LATS2* has been deleted (Murakami et al., 2011), we confirmed the endogenous interactions between TEAD4 and phosphorylated Smad3. TGF-β treatment further increased the amount of p-Smad3 that was immunoprecipitated with TEAD4 (Fig. 4 D). Consistent with the aforementioned results, interaction between endogenous Smad2/3 and YAP was observed under the existence of TEAD4 protein in Y-MESO-27 cells (Fig. 4 E). We also examined whether Smad3 and p300 augment YAP–TEAD4 complex formation and found that neither Smad3 nor p300 affects the interaction between YAP and TEAD4 (unpublished data). These data suggest that YAP, Smad3, p300, and TEAD4 mutually assist each other to strengthen the formation of a complex based on the stable binding between YAP and TEAD4 on the *CTGF* promoter.

Maximum transcriptional activation of *CTGF* promoter was observed when two proteins were overexpressed under TGF-β treatment (Fig. 4 F). Transfection of TEAD4 instead of YAP did not enhance the transactivation (unpublished data), suggesting that YAP is a prerequisite for YAP–TEAD4–Smad3–p300 complex formation and CTGF activation. We then assessed the significance of the YAP–Smad3 association in this complex. YAP-ΔCC enhanced the transactivation of the *CTGF* promoter to the same extent of full-length YAP, whereas YAP-ΔWW substantially reduced this activity, indicating that YAP–Smad3 binding plays a functionally important role in this complex (Fig. 4 G). Consistent with the presented results, the chromatin immunoprecipitation (ChIP) assay of *CTGF* promoter demonstrates that TGF-β stimulates the binding of endogenous Smad2/3 and p300 to the *CTGF* promoter but not the binding of YAP and TEAD4, which perhaps constitutively reside on the promoter region in MSTO-211H cells (Fig. 4 H). Furthermore, ChIP-reChIP assay using TGF-β–treated MSTO-211H cells showed that YAP, Smad2/3, and TEAD4 reside on the same *CTGF* promoter site (Fig. 4 I). Collectively, these data demonstrate that YAP–TEAD4–Smad3–p300 complex formation on the *CTGF* promoter is crucial for *CTGF* gene expression in MM cells.

CTGF regulates proliferation and ECM production in MM cells in vitro

Given the synergistic activation of the *CTGF* gene by both the Hippo pathway and TGF-β signaling in MM cells, we investigated whether CTGF is essential for the oncogenic properties of these cells. Using an shRNA lentiviral vector system, we examined whether CTGF is required for cell growth in NCI-H290 cells. Knockdown of CTGF suppressed NCI-H290 cell growth to a mean of 77.2% (ShCTGF#1) and 84% (ShCTGF#2), respectively, compared with the growth of the nontarget control (Fig. 5 A). We examined whether the expression of CTGF could modulate foci formation in NCI-H290 cells. Interestingly, CTGF expression showed the same response as the constitutive activation of the TGF-β type I receptor, which showed aggressive formation of foci, whereas the knockdown of CTGF reduced the number of foci (Fig. 5 B). Furthermore, the soft agar colony formation assay showed a reduction in size (Fig. 5 C, left) and the number of colonies in CTGF–knocked down NCI-H290 cells (Fig. 5 C, right). We then assessed whether CTGF expression affects the level of ECM proteins.

There is a study that shows the CTGF protein involvement in attenuation of fibronectin and Collagen 1 production induced by TGF-β in cultured human peritoneal mesothelial cells (Xiao et al., 2010). To confirm whether this CTGF function was also observed in MM cells, we used NCI-H290 cells and found that the CTGF expression affected the mRNA level of *fibronectin* and *COL1A1* in 24 h. As shown in Fig. 2, these two genes were late response genes to TGF-β, showing that CTGF modulates the expression level of ECM proteins as a consequence of a series of signaling (Fig. 5 D). The knockdown of CTGF expression abolished the aggressive formation of foci induced by the constitutively activated TGF-β type I receptor (Fig. 5 E).

CTGF is an important modulator of MM cell growth and deposition of ECM

Immunohistochemical analysis using nine human MM cells implanted into the thoracic cavity of nude mice again showed clear nuclear staining of p-Smad2, with little staining in stromal or normal tissues (Fig. 6 A, left). Nuclear staining of YAP was also observed in most tissues, although staining varied widely from weak to strong and showed a moderate correlation with the cytoplasmic staining of CTGF in MM cells (Fig. 6 A, right). Of note, the amount of stroma, which plays an important role in the cancer microenvironment, also appeared to strongly correlate with CTGF expression in MMs, suggesting that CTGF regulates the growth of MMs and also leads to a tumor environment suitable for their growth.

Based on the aforementioned findings implicating TGF-β signaling and CTGF in MM cell and tumor growth, we determined whether inhibition of TGF-β type I receptor signaling and CTGF expression induces growth suppression of MM tumors in a mouse model. SD-208 is an orally bioactive TGF-β type I receptor kinase inhibitor previously shown to significantly reduce osteolytic lesions in breast cancer bone

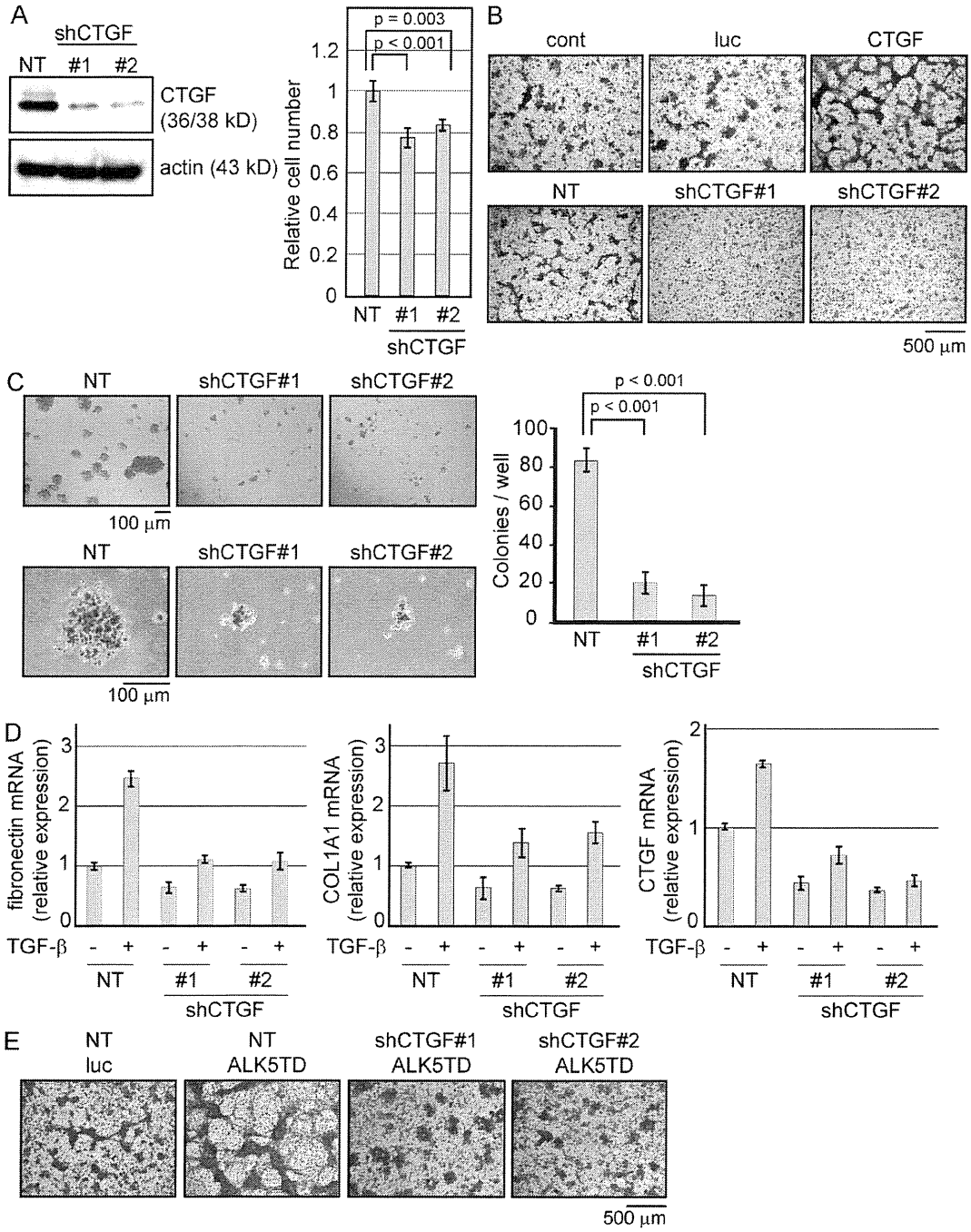

Figure 5. CTGF expression affects the growth and malignancy of MM cells. (A) NCI-H290 cells were lentivirally infected with shRNA against CTGF (shCTGF). Cell proliferation analysis was performed 4 d after lentiviral shRNA transduction. The endogenous protein level of CTGF was confirmed by Western blotting (left). Cell number was counted and normalized to the nontarget (NT) control (right). (B) NCI-H290 cells were infected with the indicated lentivirus expression vectors and stained with Giemsa after 14 d. HA-tagged luciferase (luc) was used as a control for CTGF and nontarget control for shCTGF. The results shown are representative of three independent assays. (C) Soft agar colony formation assay was performed using shRNA lentivirus-transduced NCI-H290 cells and stained with 0.5 mg/ml p-iodonitrotetrazolium after 10 d. The lower panel shows the mean size of colonies in each well. Colony number was counted in a range with a >100-μm diameter. (D) Real-time RT-PCR was performed using NCI-H290 cells infected by shRNA lentivirus 24 h after the treatment of TGF-β. (A, C, and D) Results are expressed as mean ± SEM and are representative of three independent assays. (E) NCI-H290 cells infected with the shCTGF lentivirus were kept under puromycin selection. Cells were then infected with the ALK5 lentivirus and stained using Giemsa after 14 d. The results shown are representative of three independent assays.

metastasis (Dunn et al., 2009). Oral gavage with 60 mg/kg SD-208 decreased the p-Smad2 level in NCI-H290 tissues implanted in the thoracic cavities of nude mice and further prolonged their survival (Fig. 6 B). Knockdown of CTGF expression in NCI-H290 cells also facilitated longer survival of mice (Fig. 6 C). These data demonstrate that the blockade of TGF-β signaling and suppression of CTGF protein expression impair MM tumor growth.

To further examine the contribution of CTGF expression in MM tumor growth, immunohistochemical staining was again performed by staining the 24 tissue specimens used earlier (Fig. 1 A) with YAP and CTGF antibodies. Although p-Smad2 nuclear staining was observed in all MM tumor tissues, strong CTGF expression in the cytoplasm of MM cells was dominantly observed in sarcomatoid tumors but was weak in epithelioid tumors and normal mesothelial cells (Fig. 6 D and Table 2). YAP nuclear staining was also observed in sarcomatoid tumors but was not dominant in epithelioid and normal cells, although there was a strong staining in cytoplasm in epithelioid tumor cells (Fig. 6 E and Table 2). Sporadic nuclear staining of YAP was observed in reactive mesothelioma, but compatible with the previous study which shows the amplification of *YAP* oncogene (Yokoyama et al., 2008). YAP staining in mesothelioma tissues was much stronger than normal tissues. 7 out of 12 epithelioid tissues were positively stained for YAP, suggesting that some additional factor that is present in sarcomatoid tumors might be required for CTGF expression.

Sarcomatoid mesotheliomas are composed of spindle cells with abundant stroma that resemble the histological appearance of Y-MESO-27 and NCI-H2052 cells implanted in mice (Figs. 1 A and 6 A). In MM tumor patients, histological subtype is one of the most important predictors of survival and in the selection of appropriate treatment. Our findings revealed a strong association between MM cell growth and TGF-β signaling, partially through synergistic enhancement of CTGF expression with YAP. Furthermore, we identified the involvement of CTGF in subsequent induction of stroma in MM tumors and its possible association with malignancy. Based on these findings, TGF-β and CTGF are strong candidates for targeting therapies that may be effective for both MM cells and the surrounding stroma.

DISCUSSION

MM is a cancer that often shows dissemination and progression in the thoracic or peritoneal cavity at diagnosis, and many problems remain unresolved regarding its early diagnosis and effective treatment. MM shows resistance to conventional chemotherapies probably because it does not originate from the epithelial cells and does not have the same characteristics as these cells, which can be treated with drugs. Although patients with MM usually have a poor clinical prognosis, both basic and clinical studies are lacking compared with the studies on other malignancies. Thus, there is an urgent need to develop new therapies. Based on a previous study concerning TGF-β secretion from MMs into pleural fluid and the sensitivity of murine mesothelioma to TGF-β type I receptor kinase inhibitor (Suzuki et al., 2007), we speculated a strong association between MM growth and TGF-β signaling. Moreover, MM is usually accompanied by a thick fibrotic layer that may cause thickening of the pleura and subsequent functional disorder of the lung. Because TGF-β is known to contribute to fibrosis through the Smad3-dependent pathway (Roberts et al., 2006), this fibrotic change in MM tissues could also be primarily induced by TGF-β activation. If TGF-β was continuously produced by MM tumors, TGF-β might further affect the surrounding cancer environment including fibrosis, vascularization, and suppression of immune responses. In our study, TGF-β treatment could successfully activate the Smad2/3 pathway in both normal MeT-5A and malignant MM cells, suggesting that TGF-β signaling is intact during the progression of malignancy.

One of the major categories of the TGF-β–responsive genes commonly up-regulated in both MeT-5A and Y-MESO-27 cells were ECM-related proteins that may provide anchorage for cells, making malignant cancer cells more aggressive (Radisky and Radisky, 2007; Levental et al., 2009). Furthermore, p-Smad2 nuclear staining was observed in all human MM tissue specimens, regardless of histological subtype, and also in reactivated normal mesothelial cells in MM patients, which may be evidence that constitutive activation of TGF-β signaling is a common feature during tumor development. Blockade of the TGF-β pathway in MM cells resulted in growth suppression both in vitro and in vivo. These data strongly support the hypothesis that TGF-β–stimulated growth is an innate property of mesothelial cells, which is conserved during the progression of malignancy.

Because at least 75% of MM tumors have a disturbance in the Hippo signaling pathway, this type of tumor mostly relies on this pathway for oncogenesis, whereas only 20–25% of MM tumors have a p53 mutation, which is the most frequently inactivated tumor suppressor gene in human malignancies (Sekido, 2010). Although many types of cancer cells have been recently reported to exhibit a disturbance in the Hippo signaling pathway, MM tumors have an extremely high frequency of disturbance in this pathway, indicating that the Hippo signaling pathway is the main tumor suppressor in these cells. Therefore, we investigated a possible functional link between the TGF-β and Hippo signaling pathways in mesothelioma genesis. Determining the cross talk between distinct pathways is important when searching for suitable targets of molecular target therapies because a blockade in one pathway might be insufficient to obtain the maximum effect. If there are some strong growth-driving target genes that overlap the two distinct pathways, these genes could play an important role in mesothelioma cells.

A previous study has shown that TAZ/YAP regulates the localization of Smad2/3 in response to cell density during embryogenesis (Varelas et al., 2008). TAZ/YAP dephosphorylation drives the nuclear accumulation of TAZ/YAP and Smad2/3 in the nucleus. Our data show that the two pathways also converge to regulate the transcription of disease-related target genes in MM and further relate to promote malignancy.